

Dynamic reorganization of neuronal activity Patterns in Parietal cortex

A dissertation presented

by

Laura Nicole Driscoll

to

The Division of Medical Sciences

in partial fulfillment of the requirements

for the degree of

Doctor of Philosophy

in the subject of

Neurobiology

Harvard University

Cambridge, Massachusetts

June 2017

©2017 Laura Nicole Driscoll

All rights reserved.

Dynamic reorganization of neuronal activity Patterns in Parietal cortex

Abstract

Neuronal representations change as associations are learned between sensory stimuli and behavioral actions. However, it is poorly understood whether representations of learned associations stabilize or continue to change following learning. We tracked the activity of posterior parietal cortex neurons for a month as mice stably performed a virtual-navigation task. The relationship between the activity of neurons and task features was reliable within single days, but often changed over weeks. The pool of neurons which were informative about task features (trial type and maze locations) differed across days, with change accumulating over time. Despite changes in individual cells, the population activity had statistically similar properties on each day and stable information could be decoded for over a week. As mice learned additional associations, new activity patterns emerged in the neurons used for existing representations without drastically affecting the rate of change of these representations. We propose that dynamic neuronal activity patterns could balance plasticity required for learning with stability for memory.

posterior parietal cortex (PPC)

Table of contents

Abstract	iii
List of figures	ix
Acknowledgments	x
1 General introduction and background	1
1.1 The memory engram and fixed representations in cortex	3
1.2 Synaptic plasticity and dynamic representations in cortex	4
1.3 A dynamic brain	5
1.4 Adult cortical neurons maintain flexibility	5
1.5 Tracking the activity of cells over days	7
2 Development of methods for tracking neurons and behavior over days	9
2.1 Introduction	9
2.1.1 Two photon microscopy	10
2.1.2 Fluorescent indicators	11
2.1.3 Developments in image processing	13
2.1.4 Surgical methods for optical access to brain tissue	14
2.1.5 The mouse as a model organism	15
2.1.6 A virtual reality system for mouse behavior	15
2.1.7 Posterior parietal cortex	16
2.2 Detailed methods for chronic recordings	19
2.2.1 Mice	19
2.2.2 Virtual environment design	19
2.2.3 Fixed association decision task	20

2.2.4	Training procedure	20
2.2.4.1	2 cue task training	21
2.2.4.2	3 and 4 cue task training	22
2.2.4.3	Bias correction	23
2.2.5	Surgical procedures	23
2.2.6	Field sign maps	24
2.2.6.1	Widefield microscope design	24
2.2.6.2	Visual stimulus design	25
2.2.6.3	Retinotopy analysis design	25
2.2.7	Two photon microscope design	26
2.2.8	Image acquisition	26
2.2.9	Processing of imaging data	27
2.2.10	Within-session processing	28
2.2.11	Across-session processing	29
3	Dynamic reorganization of neuronal activity patterns in parietal cortex	33
3.1	Introduction	33
3.2	Results	34
3.2.1	Tracking behavior and neuronal activity over weeks	35
3.2.2	Necessity of PPC activity for post-learning performance of the task . .	37
3.2.3	Reorganization of sequential activity across maze locations	39
3.2.4	Different populations of neurons with trial type-specific activity patterns across days	40
3.2.5	Using a generalized linear model to compare relationships between neuronal activity and behavioral features across days	44
3.2.6	Changing activity-behavior relationships in single neurons over days .	51
3.2.7	Consistent statistical features of population activity on each day	59
3.2.8	Decoding of information from dynamic neuronal representations	60
3.3	Discussion	65
3.4	Acknowledgements	66

3.5 Author contributions	66
3.6 Data analysis methods	67
3.6.1 General analysis procedures	67
3.6.2 Identification of significant peaks of activity	68
3.6.3 Encoding model	68
3.6.3.1 Model parameters	69
3.6.3.2 Fitting	70
3.6.3.3 Analysis of model	71
3.6.3.4 Metric of consistency in activity-behavior relationships	73
3.6.3.5 Contribution of task and behavioral features to the activity of a cell	74
3.6.4 Decoding	74
4 Monitoring neuronal activity over days during learning	76
4.1 Introduction	76
4.2 Results	76
4.2.1 Task design for learning a stimulus-action pair	76
4.2.2 Rate of change during learning compared to stable behavior	77
4.2.3 Neurons with novel cue related activity	79
4.3 Discussion	80
4.3.1 Trial-trial variability is stable over learning	81
4.3.2 Steady number of task related neurons during learning	83
4.4 Methods	84
4.4.1 Dimensionality reduction of neuronal and behavioral data	84
4.4.2 Cosine distance	85
5 Discussion and future experiments	86
5.1 Dynamic reorganization of activity in cortex	86
5.2 A strategy for maintaining and updating relevant activity patterns	87
5.3 Balancing stability and flexibility according to role	89
5.4 Stability in the emergent properties of the network	90

References	102
-------------------	------------

Listing of figures

2.1	PPC relative to retinotopic maps	18
2.2	Cell identification protocol across days and number of samples for various day comparisons	31
2.2	(Continued)	32
3.1	Chronic imaging during stable performance of a virtual-navigation decision task.	36
3.2	Neuronal population dynamics and inactivation experiments.	38
3.3	Reorganization of activity within a trial across days.	41
3.4	Reorganization of information about trial-type across days	43
3.5	GLM fitting procedure	46
3.6	Basis functions for encoding model.	47
3.6	(Continued)	48
3.7	Fitting activity-behavior relationships with a generalized linear model.	50
3.8	Fitting activity-behavior relationships with a generalized linear model.	52
3.9	Behavioral features were variable but had overlapping distributions across days	53
3.10	Model comparison across days.	53
3.11	Quantification of consistent, lost and gained activity-behavior relationships. .	55
3.12	Distribution in the rate of change across cells in the population.	58
3.13	Behavioral change across days does not explain neuronal change.	59
3.14	Stable statistical features of population activity.	61
3.15	Decoding task information across days.	63
4.1	Neuronal activity during learning of a novel trial type	77
4.2	Differences in activity between trial types.	78

4.4 Neurons with novel cue related activity came from the pool of cells with recent familiar cue related activity.	80
--	----

Acknowledgments

shout out to the homieszzz

Chapter 1

General introduction and background

A major function of neurons in the cortex is to form associations between stimuli in the sensory environment and behavioral actions. In some cases these associations can be formed between arbitrary stimuli and responses, such as, for example, when learning to relate landmarks in an environment with navigation actions or when learning behaviorally-relevant categories of sensory cues (Freedman & Assad, 2016; Harvey et al., 2012). These associations are mediated by patterns of neuronal activity that develop through the course of learning (Freedman & Assad, 2006). Past work has studied these patterns to understand how sensorimotor associations are represented in cortical neurons. Nearly all this work has focused on measurements of neuronal activity at single snapshots in time. For example, in typical experiments, activity from one neuron or set of neurons is recorded on one day and activity from other neurons is recorded on subsequent days. Information about sensorimotor associations is thus built up based on snapshots from different sets of neurons measured at separate time points. A fundamental question therefore remains unanswered: does neuronal activity converge to a stable pattern following learning or does neuronal activity change even after expert performance has

been achieved on a learned task? The answer to this question is essential to understand how sensorimotor associations are represented in cortex.

Here we tested if cortical representations of learned associations between arbitrary stimulus-action pairings stabilized after these associations had been learned to expert levels. We also tracked the same neurons during learning of novel stimulus-action pairs and compared change during learning to change during stable behavioral performance. We developed methods to track the activity of populations of neurons and behavioral patterns across weeks as mice performed a navigation-based decision task in virtual reality. We focused on activity in the posterior parietal cortex (PPC), which is essential for performing this task and in rodents is considered to function in learned sensorimotor associations, including during navigation (Harvey et al., 2012; McNaughton et al., 1994; Nitz, 2006; Whitlock et al., 2012). We found that activity patterns in individual neurons changed greatly over the course of days and weeks, such that the population of neurons that provided the most task-relevant information drifted over time. Despite changes in single cells over time, the PPC population maintained a steady state with the same statistics of population activity properties across weeks, such as, for example, a consistent distribution of the fraction of neurons active at each point in the trial. Information about the task could be decoded above chance for several days using a fixed decoder, indicating that a stable readout of population activity could exist, despite changes in individual neurons. Also, representations of newly learned cue-response relationships were incorporated without perturbing existing representations. We propose that drift in neuronal activity patterns could be important for mediating a tradeoff between

stable encoding of information and flexibility for incorporating new information.

In this chapter we review a history of studies that characterize learned population representations in cortex. In chapter two we discuss recent technological advances that allow tracking of the same population of hundreds of neurons with single cell resolution over several weeks. Chapters three and four outline our key findings, describing instability of representations after learning and during learning respectively. In chapter five we discuss the implications of our findings and propose future studies to address questions that arise from this work.

1.1 The memory engram and fixed representations in cortex

A common framework for memory proposes that there is a direct and fixed mapping of neuronal activity patterns with sensory stimuli and behavioral actions. In this framework, learned associations are thought to develop through the linking of these fixed representations (Messinger et al., 2001; Sakai & Miyashita, 1991; Veit et al., 2015). During learning, synaptic and other biophysical changes are thus hypothesized to minimize errors in the link between sensory stimuli and behavioral outputs, eventually converging to a stable solution upon reaching expert performance on a task (Ganguly & Carmena, 2009; Peters et al., 2014; Chestek et al., 2007). This view proposes that a memory engram is a collection of the same neurons that are activated every time the learned association is recalled (Tonegawa et al., 2015). This framework is appealing due to its conceptual simplicity and because artificial networks that converge to a fixed

mapping of inputs to outputs through learning have proven highly successful in solving complex tasks (Abbott & Sussillo, 2009; Buonomano, 2005; LeCun et al., 2015). This framework for learned representations in cortex requires careful maintenance of the synaptic partners, intrinsic firing rate properties and response properties for single cells. In a massive recurrently connected network where change in the response properties of a small number of neurons could snowball, this careful maintenance of single neuron response properties poses a great challenge.

1.2 Synaptic plasticity and dynamic representations in cortex

Alternatively, experimental data have revealed that synaptic connections between neurons in various brain regions continually change over time, with only a small fraction of synaptic connections, and in some cases none, persisting over weeks and months (Attardo et al., 2015; Stettler et al., 2006; Trachtenberg et al., 2002). These results have motivated theoretical models that propose continuous change in neuronal circuits as a mechanism to optimize a tradeoff between stability and flexibility by sampling from multiple solutions of activity patterns and connectivity that similarly convey relevant information (Ajemian et al., 2013; Kappel et al., 2015; Rokni et al., 2007). These models present computational benefits such as limiting the likelihood of overtraining and convergence to local optima.

1.3 A dynamic brain

Synaptic stability and plasticity in a floating world AMPA Receptor Trafficking at Excitatory Synapses Roger A Nicoll

1.4 Adult cortical neurons maintain flexibility

Early demonstrations of flexibility in cortical neuron representations were made through perturbations in ocular dominance in the visual cortex of cats. Susceptibility of cortical neuron responses to eye suturing were measured at various stages throughout development. These experiments revealed a brief window of time, early in development, where recovery was optimal. The idea of a critical period led to the expectation that all connections and functional properties in sensory areas were fixed later in life (Gilbert & Wiesel, 1990). Decades later, experience dependent alterations in receptive field properties were demonstrated in adult animals through lesions in sensory organs. After lesion experiments, cortical neurons in the lesion projection zone (the target cortical region for amputated sensory inputs) became silent and later acquired the receptive field of surrounding neurons (Merzenich et al., 1984; Robertson & Irvine, 1989; Kaas et al., 1990). Similar experiments in the motor system produced a corresponding result. When the facial nerve of the rat was cut, the area of motor cortex driving this muscle developed control over forelimb or eye musculature instead (Gilbert & Wiesel, 1992). This process is believed to occur through competition between synaptic inputs of neighboring

horizontally projecting cortical neurons and thalamocortical inputs. When thalamic neurons no longer receive sensory input and become silent, horizontal projections from neighboring cortical neurons take over (Darian-Smith & Gilbert, 1994).

This type of structural plasticity was later shown to be unnecessary for drastic changes in the tuning properties of neurons in visual cortex. A single monocular deprivation episode early in life produced enhanced plasticity later in life during a second monocular deprivation (Hofer et al., 2006, 2009). A mechanism for this phenomenon was proposed where early structural changes in horizontal connections were maintained later in life that could be exploited to facilitate rapid recovery after the second monocular deprivation. Rather than requiring energetically costly structural change, this second monocular deprivation could simply induce fine tuning changes of existing connections. This mechanism for rapid re-learning through fine tuning of existing connections could provide the molecular basis for 'savings', a term used in psychology to describe the elevated rate of re-learning compared to an original learning event (Ebbinghaus, 1880). This work also suggests major changes in response properties are possible without structural change. Given these drastic changes are possible simply through fine adjustments to existing synapse strength, combined with the reported rate of structural change throughout adulthood, it appears likely that neuron response properties are prone to modification.

Together, this work demonstrates the ability of adult cortical neurons to dynamically reorganize their response properties in order to optimally represent the full range of stimuli in the animal's environment. This is a valuable network feature for the

maintenance of relevant representations of a changing environment.

1.5 Tracking the activity of cells over days

In many areas of cortex in the rodent brain, neighboring neurons exhibit a wide range of tuning properties for various behaviorally relevant stimuli. Given that adult cortical neurons reportedly take on the response properties of their neighbors in the absence of thalamic input, it will be important to measure the degree to which neighboring neurons exchange tuning properties during steady-state behavior, in the absence of perturbation. The degree to which tuning profiles of individual cells change during and after learning remains unclear.

Recently developed methods to track the activity of the same neurons over time have led to a growing body of literature examining how representations change with learning (Huber et al., 2012; Komiyama et al., 2010; Peters et al., 2014; Poort et al., 2015). However, relatively little work has examined the stability of these representations after learning. Pioneering studies have investigated the stability of representations of sensory stimuli or the patterns of activity that accompany motor actions, in most cases over the course of several days. Studies in sensory cortex have revealed that representations of basic stimulus features, such as visual stimulus orientation, are generally stable over the examined periods (Tolias et al., 2007; Andermann et al., 2010; Mank et al., 2008; Margolis et al., 2012; Peron et al., 2015b; Poort et al., 2015; Rose et al., 2016) . In motor cortex, the stability of activity patterns for generating motor actions is a controversial topic. Many studies have noted stability in motor cortex activity but some have identified

subtle shifts in tuning over days (Chestek et al., 2007; Ganguly & Carmena, 2009; Huber et al., 2012; Peters et al., 2014; Padoa-Schioppa et al., 2004; Rokni et al., 2007; Stevenson et al., 2011). Also, a recent study has reported a mix of stable and changing features in the activity in songbird HVC during the generation of learned birdsong (Liberti et al., 2016). The largest changes in neuronal activity patterns over time have been noted in the hippocampus, in which upon repeated exposure to the same environment, place cell activity was gained and lost in individual cells without apparent shifts in place field locations (Kentros et al., 2004; Ziv et al., 2013). This work was performed in the absence of a task that required hippocampal activity and results have in part been attributed to learning and forgetting of environments (Attardo et al., 2015; Ziv et al., 2013). Therefore, the emerging literature on the stability of neuronal activity patterns over time provides hints that a degree of instability may exist. However, no studies have shown a major reorganization of activity patterns that are required for a learned behavior, leaving open the possibility that any instabilities noted might not be relevant for key features of behavioral output. In addition, much work has been limited by the available methods to confidently track neurons across days because it is difficult with electrophysiology or with supra-cellular resolution epifluorescence imaging to provide reliable metrics of cell identities on each day (Peron et al., 2015a).

Chapter 2

Development of methods for tracking neurons and behavior over days

2.1 Introduction

Significant technical limitations have prevented direct measurements of single cell activity-behavior relationships over long timescales, during stable behavior and during learning. To study how single cell response properties are modified or maintained over days and weeks, it is necessary to 1) measure the activity of the same neurons over time, 2) to do this in a behaviorally-relevant context, that is during a behavioral task. Recent technical advances in optical recording methods and head-fixed behavioral task design have satisfied these experimental demands.

Optical recording methods are additionally advantageous compared to electrical recording methods as they are more comprehensive and less invasive. Our brain region of interest, cortex, is located on the surface of the brain, thus optical access can be achieved in the intact brain. Compared to single or multiunit electrodes, this method is far less invasive,

which will be important for long term recordings where tissue damage may cause changes in neuronal response properties. Optical recording methods are more comprehensive as a larger area of neurons may be recorded simultaneously. Additionally the experimenter can identify the fraction of active neurons using optical methods, whereas in electrical recordings silent neurons are missed. Although we didn't take advantage of cell type information in these studies, additional information using genetic markers can be incorporated into future work through the use of additional fluorescent markers.

2.1.1 Two photon microscopy

The development of multi-photon fluorescence microscopy has allowed for high resolution, high sensitivity measurement of fluorescent probes in light scattering tissue, up to 1 mm deep (Denk et al., 1990; Oheim et al., 2001; Theer et al., 2003). This system works through the combination of two low energy photons exciting one fluorescent molecule simultaneously, resulting in a transition to a higher energy state and a higher energy emission than would be possible from a single photon. This type of absorption scales with the second power of the light intensity, which drops off quadratically above and below the focal plane. As a result this is a nonlinear process, providing high resolution excitation within $\approx 0.1 \mu\text{m}^3$ (Zipfel et al., 2003). The use of low energy excitation light lessens the extent of photodamage in the tissue and allows for deeper penetration of excitation light due to reduced levels of scattering. Light is scattered in the tissue throughout both the excitation path and the emission path (half of photons are scattered every 50-200 μm (Oheim et al., 2001; Yaroslavsky et al., 2002). Light scattered

on the excitation path reduces light intensity in the focal region, but doesn't result in off-target excitation due to the low probability of two scattered photons simultaneously hitting the same fluorescent probe. Therefore, the source of all collected emission photons is the focal excitation volume and can be incorporated into the signal. This combination of high resolution excitation and blanket emission signal contribution allows high resolution and high sensitivity measurement of fluorescent probes in light scattering tissue.

2.1.2 Fluorescent indicators

More recent developments in fluorescent probes for neuronal activity have dramatically improved the signal strength and temporal resolution of optical recording methods. The local concentration of calcium ions rises between 10 and 100 fold in the soma during an action potential due to the opening of voltage gated calcium channels, making calcium ion concentration a good measure of activity (Berridge et al., 2000). Structure guided optimization of the calcium sensor GCaMP, the circularly permuted green fluorescent protein linked to the calcium binding protein calmodulin, has rendered this complex the most widely used calcium sensor. The latest version of GCaMP was identified through a large scale genetic screen in neurons with the aim of improving sensitivity. GCaMP6 includes three variants, differing in their sensitivity and kinetics. All of these variants, (fast, medium and slow describe the off-rate of calcium binding) are reported to identify single spikes *in vivo* with signal strength inversely proportional to their off-rate. We chose to use GCaMP6m (medium) as the signal strength is nearly as high as GCaMPs (slow), with a faster off rate. Various versions of GCaMP have already been used to detect neural

activity in large neuronal populations in the PPC (Harvey et al., 2012), visual cortex (Andermann et al., 2010), motor cortex (Komiyama et al., 2010; Huber et al., 2012; Peters et al., 2014), barrel cortex (Margolis et al., 2012; Peron et al., 2015a), and hippocampus (Ziv et al., 2013) of behaving mice. Long-term imaging of GCaMP has revealed learning-related circuit changes *in vivo* (Makino & Komiyama, 2015; Peters et al., 2014). Despite these advances, there are still limitations of these recording tools. Calcium indicators lack information about the relative event rate across neurons and blur the response timing of neurons. Calcium indicators also bias sampled activity to higher firing rates because small spike numbers can be missed.

There are two options for the induction calcium indicator expression *in vivo*: virus-based vector system and transgenic mouse lines. Long term viral expression provides superior signal to noise than current transgenic lines, although expression is variable across cells and is unstable over time, eventually leading to nuclear expression of the indicator and cell death. Transgenic lines do not have similar cell health problems and require a less invasive surgical procedure without the need for injections. However, expression levels in transgenic mice are low, resulting in poor signal to noise. Additionally one leading GCaMP6 transgenic line is reported to cause seizures in mice. Consequently, viral expression of calcium indicators is still the most widely implemented method for the induction of calcium expression. While the majority of cells display no aberrant response properties over the course of 1-2 months, careful measures must be taken to exclude unhealthy cells, which are conveniently labeled by nuclear expression of the indicator.

This feature of virally expressed calcium indicators remains a source of concern and should be considered in the interpretation of our results.

An additional fluorescent protein that provides a stable image, independent from calcium responses, is useful for image registration across a single session and for field of view alignment across days. We additionally express the red fluorescent protein tdTomato in conjunction with the calcium indicator GCaMP6m.

2.1.3 Developments in image processing

Rapid advances in these technologies require matched developments in processing methods. There are three standard steps of image processing, 1) image registration across frames, 2) segmentation of fluorescent sources and 3) deconvolution to recover spiking information. Pipelines for these steps are often designed ad hoc and are specific to the indicator and acquisition methods of individual experimenters. Image processing techniques for these data are still in infant stages, although there has been a large amount of progress in the past decade.

Two-photon excitation microscopes acquire single pixel intensities sequentially by scanning focused laser pulses across the imaging plane. Small displacements in the target tissue due to brain motion result in nonuniform distortions of the image. These distortions can often be reduced post hoc through image registration methods. Optimal registration methods incorporate statistics of acquisition methods into the design of the registration algorithm. For example, line scans result in a smaller temporal difference between

horizontally adjacent pixels than vertically adjacent pixels. The Lucas Kanade method capitalizes on this piece of information to correct for distortion within a frame. Segmentation and deconvolution methods are also developing quickly. Coordinated competitions for data processing methods with ground truth data, such as codeneuro, will be crucial for the widespread acceptance and application of verified methods.

2.1.4 Surgical methods for optical access to brain tissue

These optical tools allow unprecedented access to the most superficial brain regions, specifically cerebral cortex, literally 'brain bark'. Utilization of these tools requires the partial removal of the overlying bone. This is achieved either through thinning the bone or by permanently replacing bone with glass. Both the thinned skull and the cranial window prep can lead to inflammation and microglia activation. Careful surgical technique is required to minimize the disruption of tissue (Dorand et al., 2014; Xu et al., 2007). The cranial window surgery requires drilling down to very thin layers of bone without heating up or piercing brain tissue. The thinned skull prep is similarly difficult, where the appropriate bone thickness is 20 - 25 μm directly above the target imaging region. Chronic recordings through thinned skull are made difficult by skull irregularities, regrowth and repeated skin closure and resections. Approximately five days post-operation, bone regrowth occludes brain tissue and the skull must be repeatedly thinned up to five times total (Yang et al., 2010). As a result cranial glass windows are the most widely accepted method for tracking the activity of neurons over days (Goldey et al., 2014).

2.1.5 The mouse as a model organism

The combined advances in molecular and genetic tools and quantitative mouse behavior make mice the ideal model organism for studying neuronal population activity in relation to behavior. Careful quantitative behavior in mice is now on par with those in primates in terms of stimulus and behavioral control. A standard method in monkeys has been to head-fix and restrain the body of the animal. These methods allow careful measurement of unrestricted behavioral readouts, such as eye and arm position. New behavioral methods in rodents attempt to emulate these precision practices. A wide range of head fixed behaviors in mice have been developed over the past two decades. Mice have demonstrated perceptual capabilities for simple discrimination and decision making behaviors that have become increasingly complex. As in primate studies, mice are capable of performing hundreds of trials with performance approaching near perfect levels. Experiments in primates have laid the groundwork for quantitative analysis of neuronal activity in relation to behavior, however the development of quantitative and conceptually rich mouse behavior in conjunction with rapid advancements of mouse specific molecular tools have rendered mice the ideal organism for future work in this area (O'Connor et al., 2009; Andermann et al., 2010).

2.1.6 A virtual reality system for mouse behavior

The head fixed behavioral setup not only allows more precise stimulus control and precision measurements of motor outputs, but additionally allows implementation of advanced optical

recording techniques. We use a head fixed behavior setup for the animal as in previous in vivo imaging studies (Dombeck et al., 2010; Huber et al., 2012; Harvey et al., 2012). We use a navigational task as navigation is a natural decision making behavior for rodents. Our task employs a previously described virtual reality system (Harvey et al., 2009). The mouse's running on a spherical treadmill controls translation and rotation a virtual environment. The virtual environment is projected onto a screen in a closed loop with the movements of the mouse. Mice are able to interact with the virtual environment, rapidly increasing their reward rate often within a single imaging session.

2.1.7 Posterior parietal cortex

An ideal brain area to study learned associations is the posterior parietal cortex because the PPC links sensory representations to a behavioral response. This sensorimotor association area is likely flexible during learning of new associations between sensory inputs and a motor response. PPC receives input from primary and secondary sensory areas and has extensive reciprocal connections with prefrontal association areas, frontal regions, limbic structures, as well as superior colliculus and basal ganglia (Harvey et al., 2012; Constantinidis et al., 2004). PPC has been traditionally linked with spatial attention and movement planning (Bisley & Goldberg, 2010; Andersen & Cui, 2009). Involvement in cognitive functions such as working memory and task learning has become increasingly evident (Rawley & Constantinidis, 2009). Lesions in PPC induce spatial attention and working memory deficits in humans. Typically after a lesion in the right hemisphere, patients will experience inability to detect objects in the contralateral visual hemisphere or

to perceive the left side of objects, regardless of where they appear within the visual field. Balint's syndrome is common in PPC lesion studies where patients are unable to perceive more than one visual stimulus at a time, to direct visual attention outside the fovea, to scan visual space, or to coordinate hand movements to visual targets (Constantinidis, 2006). Another role of the PPC is its function in receiving and integrating polymodal sensory information, and transforming it into goal-directed motor movements (Seal, 1989; Stricanne et al., 1996; Batista et al., 1999). PPC is recognized for its role in motor learning and retrieval of learned complex motor skills (Gallese et al., 1994; Goodale & Milner, 1992; Haaland et al., 2000; Rushworth et al., 1998). The precise role of PPC in the decision making circuit is somewhat controversial. Initial reports of working memory activity in the posterior parietal cortex described spiking in monkey area LIP that followed the offset of a visual stimulus, which was to be a target for a planned eye movement (Barash et al., 1991). Later studies demonstrated that posterior parietal neurons represent the remembered locations of visual stimuli, independent of a planned motor response (Freedman & Assad, 2009; Constantinidis & Steinmetz, 1996; Berryhill & Olson, 2008). More recent work in rodent PPC have demonstrated a role for this association area during the cue period of visual decision making tasks, suggesting rodent PPC is involved in some form of visual processing or potentially the transformation of stimulus information into an action plan. PPC activity is working memory task modulated, linking sensory information and the behavioral response, making it an ideal focus for the study of learned cue-response relationships. This association area will serve as an example for learning and cortical

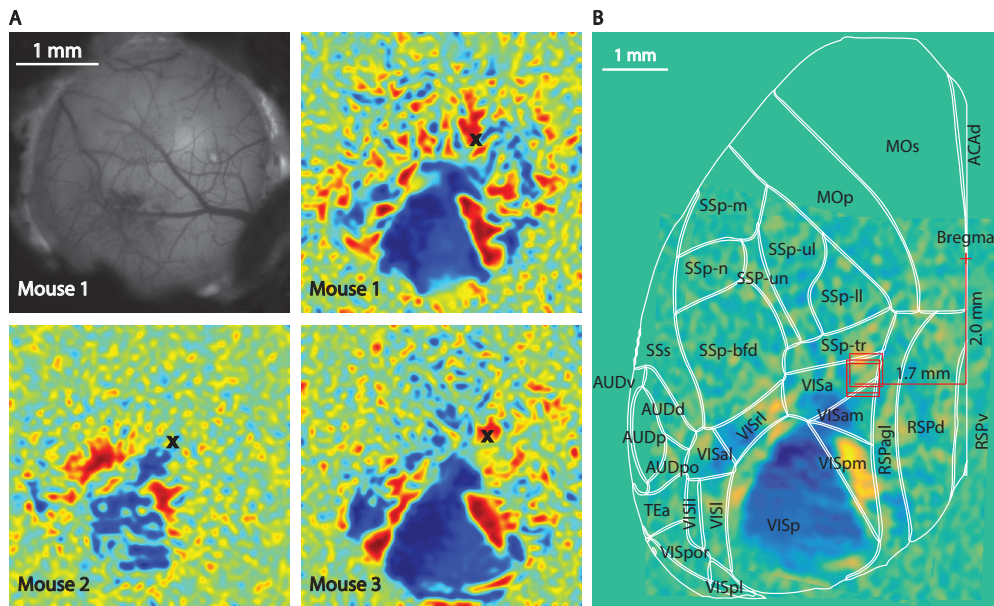


Figure 2.1 | PPC relative to retinotopic maps. a, Upper left: Blood vessel image through cranial window. Upper right and bottom panels : Field sign maps **b**, Combined field sign maps overlayed with a dorsal map of cortical areas defined by the Allen Mouse Common Coordinate Framework.

processing in other association areas.

Functionally defined boundaries for higher order visual areas is an active area of investigation (recent neuron papers). The Allen Institute Mouse Brain Atlas provides a widely accepted map of cortical areas defined by connectivity. This map has been in flux over recent years, with subtle changes in cortical area boundaries in each new addition. We define our PPC coordinates 2 mm posterior and 1.7 mm lateral of bregma. We performed retinotopic mapping experiments to identify our stereotactically defined PPC relative to functionally defined visual areas. These coordinates corresponded to a location anterior to cortical regions identified using retinotopic mapping. Here we note that recent work from the Allen Brain Institute calls this region VisA (?) and that this region is medial to what previous work has called secondary visual area A (Wang & Burkhalter, 2007).

2.2 Detailed methods for chronic recordings

2.2.1 Mice

All experimental procedures were approved by the Harvard Medical School Institutional Animal Care and Use Committee and were performed in compliance with the Guide for the Care and Use of Laboratory Animals. Three male C57BL/6J-Tg(Thy1-GCaMP6s)GP4.12Dkim/J mice were used for widefield retinotopic mapping experiments. All other data were obtained from five male C57BL/6J mice (Jackson Labs), which were 8-10 weeks old at the start of behavioral training, and 14-32 weeks old during imaging. A surgery was performed on each mouse before training to affix a titanium headplate to the skull using dental cement (Metabond, Parkell). At least one day after headplate implantation, mice began a water schedule, in which they received 800 l of water/day. Mouse health was monitored daily. Mice were given additional water if their weight fell below 80 % of their pre-schedule weight (23.2 ± 0.5 g, mean \pm sem). Mice were housed in pairs of littermates.

2.2.2 Virtual environment design

Virtual reality environments were constructed and operated using MATLAB-based ViRMEn software (Virtual Reality Mouse Engine) (Aronov & Tank, 2014; Harvey et al., 2009). A PicoP microprojector (MicroVision Inc.) projected the virtual environment onto the back side of a 24 inch diameter half cylindrical screen. The virtual environment was

updated in response to the mouse’s manipulations of an open cell Styrofoam spherical treadmill (8 inch diameter, 135 g). An optical sensor positioned beneath the spherical treadmill measured movements in pitch and roll of the ball (relative to the mouse’s body axis). These signals controlled forward/backward and rotational movement in VR, respectively. We recorded the mouse’s position in the virtual environment (x/y position), the rotational speed of the spherical treadmill (about the pitch and roll axes), and the mouse’s view angle in the environment.

2.2.3 Fixed association decision task

We trained mice to perform a two-alternative forced-choice task based on navigation through a T-maze in visual virtual reality (Harvey et al., 2012). At the beginning of the T-stem, mice saw one of two possible visual cues (white walls or black walls). Mice then ran through a short delay period portion of the T-stem in which the walls were identical between trial types. Upon reaching the T-intersection, mice had to report a choice about the cue identity by making a left or right turn to receive a reward. Mice learned this task over 4-6 weeks of training and reached expert behavioral performance that was mostly stable over weeks.

2.2.4 Training procedure

Mice were on the water schedule for at least five days before behavioral training began. Training sessions were performed daily and lasted 45-60 minutes at roughly the same time of day each day. Rewards (4 L of 10% sweetened condensed milk in water) were delivered

through a lick spout. Mice were trained to perform the T-maze task using a program of five mazes.

2.2.4.1 2 cue task training

Maze 1 was a linear track in which the mouse had to run forward to get a reward. After each trial the maze was either lengthened or shortened to maintain an approximate reward rate of 4 rewards/minute. When the mouse completed a trial in less than 15 seconds, the central corridor would grow by 10 centimeters on the next trial or shrink by the same amount if the trial was completed in greater than 15 seconds. The minimum length of the maze was 37.5 cm and the maximum was 3 m (measured as running distance on the treadmill).

In maze 2 the mice had to turn toward a tower above the left or right T-arm in the virtual world. This maze trained the mice to follow a visual cue for reward and improved running skill on the treadmill. Again, after each trial the maze was either lengthened or shortened to maintain an approximate reward rate of 4 rewards/minute with a minimum length of 70 cm and a maximum length of 3.5 m.

In maze 3, mice began to associate colored walls with the cued turn direction. When the tower was on the right, the walls were black. When the tower was on the left, the walls were white. On alternating trials we added a second tower so that there was one on each side, and the mouse had to use the wall color to plan the turn direction. Maze 3 was 4 m in length.

The delay period was gradually incorporated into maze 4, such that the cue offset (delay onset) shifted earlier in the trial. The criteria for advancement to the next maze in the sequence, on mazes 3 and 4, were a trial rate of > 4 trials/minute and > 80% correct for 2-3 consecutive days.

In maze 5, the lengths were fixed with the total length of 4.5 m and a delay period of 2.25 m. The colored walls were either black with white dots or white with black dots followed by a gray striped segment throughout the delay period that was identical across trial types. The entire training program was completed in 4-8 weeks.

2.2.4.2 3 and 4 cue task training

Training for novel trial type associations was performed during imaging. Mazes were identical to maze 5. On each day, mice were presented with novel trial types after 40 trials of the original trial types (black cue-right turn and white cue-left turn). After novel trial types were introduced, familiar trial types and novel trial types were interleaved such that there were equal fractions of left and right turn trials. Mice were first presented with a 3rd cue (crosshatch) and after mice performed all three trial types at above 80% for three consecutive days, we introduced a 4th cue (triangles). For mouse 1, the 3rd cue instructed left turns and the 4th cue instructed right turns. For mouse 3, the cue-turn relationship for novel trial types was reversed. White and black cues maintained consistent cue-turn relationships for both mice. Mice learned novel trial type cue-turn relationships by trial and error while maintaining previously learned relationships for black and white cues.

2.2.4.3 Bias correction

Some mice developed biases during training such that left or right turns were favored. During training, we implemented a bias correction. On each trial, the probability that a mouse would be presented with a left turn trial was the fraction of times the mouse turned right on the previous 20 trials. Once mice reached expert levels, biases were rare and bias correction was unnecessary. Bias correction was not used during imaging sessions.

2.2.5 Surgical procedures

After mice achieved performance greater than 80% correct on the task for five consecutive days, they received ad lib access to water for three days before the cranial window implant surgery. A circular craniotomy with a diameter of 3.1 mm was made over left PPC (stereotaxic coordinates: 2 mm posterior, 1.7 mm lateral of bregma). Three 10 nL injections of a virus mixture containing a 4:1 volumetric ratio of tdTomato (AAV2/1-CAG-tdTomato) to GCaMP6m (AAV2/1-synapsin-1-GCaMP6m) (University of Pennsylvania Vector Core Facility) were made near the center of the craniotomy at a depth of 275 μ m below the dura. Injections were slow (5 min/injection) and continuous (custom air pressure injection system). The pipette (15 μ m tip diameter) was advanced using a micromanipulator (Sutter MP285) at a 30-degree angle relative to horizontal to minimize compression of the brain. A glass plug consisting of a single 5 mm diameter coverslip on top of two 3 mm diameter coverslips (# 1 thickness; CS-5R and CS-3R, Warner Instruments) were combined using UV-curable optically transparent adhesive

(Norland Optics) and were affixed to the brain with minimal Kwik-Sil (World Precision Instruments) and affixed to the skull using Metabond on the perimeter of the 5mm coverslip lip. The metabond mixture contained 5% vol/vol India ink, to prevent light contamination from the VR display. A titanium ring was mounted on top of the headplate. This ring interfaced with the objective lens through a cylinder of black rubber, to prevent light contamination (Dombeck et al., 2010). Mice resumed training after at least one day of recovery. Imaging began at least three weeks post-injection and was continued for up to 8 weeks. On a given day, we imaged 100 - 300 neurons simultaneously during approximately 200 trials.

2.2.6 Field sign maps

To visualize Bregma guided PPC coordinates relative to the retinotopic map in visual areas of the mouse cortex, we performed widefield imaging in GCaMP6s transgenic mice (C57BL/6J-Tg(Thy1-GCaMP6s)GP4.12Dkim/J) during a stimulus protocol for retinotopic mapping.

2.2.6.1 Widefield microscope design

Retinotopic mapping was performed with a tandem-lens epifluorescence macroscope (Ratzlaff & Grinvald, 1991). Excitation light (455 nm LED, Thorlabs) as filtered (469 nm with 35 nm bandwidth, Thorlabs) and reflected onto the brain through an inverted camera lens (NIKKOR AI-S FX 50 mm f/1.2, Nikon). Emission light was collected by the same lens, emission-filtered (525 nm with 39 nm bandwidth, Thorlabs), and imaged by a second

camera lens (SY85MAE-N 85 mm F1.4, Samyang) onto a CMOS camera (ace acA1920-155um, Basler). Images were collected at 60 Hz, synchronized to the visual stimulus presented on a gamma-corrected 27 inch IPS LCD monitor (MG279Q, Asus).

2.2.6.2 Visual stimulus design

Stimulation was performed as described in (Marshel et al., 2011). The monitor was placed in front of the right eye at an angle of 30 degrees from the mouse's midline. The stimulus was a black and white checkered moving bar on a gray background, corrected to have constant width (5 degrees) and speed (7 degrees per second) in spherical coordinates centered on the mouse's eye as described in (Marshel et al., 2011). The stimulus was presented in blocks containing 6 repeats of each of four movement directions (up, down, forward, backward). 6 blocks were presented per session.

2.2.6.3 Retinotopy analysis design

Retinotopy was determined by computing the temporal Fourier transform at each pixel and extracting the phase at the frequency of stimulus presentation, as described in (Kalatsky & Stryker, 2003). The phase images were averaged across all trials of the same orientation and smoothed using a Gaussian kernel with standard deviation $30 \mu\text{m}$ to obtain horizontal and vertical retinotopic maps. The field sign map was then calculated as the sine between the gradient angles of the horizontal and vertical retinotopic maps (Garrett et al., 2014; ?). Field sign maps were aligned to Allen Institute field sign maps using control point registration and overlaid with a dorsal map of cortical areas defined by the Allen Mouse

Common Coordinate Framework (?)

2.2.7 Two photon microscope design

Data were collected using a custom-built two-photon microscope. A resonant scanning mirror and galvanometric mirror separated by a scan lens-based relay telescope on the scan head allowed fast scanning. A Olympus 25x 1.05 NA objective lens was mounted on a piezo collar (Physik Instrumente) that allowed slower axial scanning. An aluminum box housed collection optics to block light interference from the VR display. Green and red emission light were separated by a dichroic mirror (580 nm long-pass, Semrock) and bandpass filters (525/50 and 641/75 nm, Semrock) and collected by GaAsP photomultiplier tubes (Hamamatsu). A Ti:sapphire laser (Coherent) delivered excitation light at 920 nm with an average power of about 35-70 mW at the sample. The microscope was controlled by ScanImage (version 4; Vidrio Technologies) (Pologruto et al., 2003). The spherical treadmill was mounted on an XYZ translation stage (Dover Motion) to position the mouse under the objective.

2.2.8 Image acquisition

Four imaging planes were acquired by volumetric scanning at 5.3 Hz with a resolution of 512 x 512 pixels ($500 \mu\text{m} \times 500 \mu\text{m}$) for each plane. Planes were separated by $25 \mu\text{m}$ axially between 120 and $250 \mu\text{m}$ below the dura. Imaging was continuous over behavioral sessions lasting 45 minutes to 1 hour. Bleaching of GCaMP6m was negligible over this time. Approximately every 20 minutes, slow drifts of the field of view were manually

corrected using comparison to a reference image. The imaging frame clock and an iteration counter in ViRMEn were recorded to synchronize imaging and behavioral data.

2.2.9 Processing of imaging data

One field-of-view was acquired for each of the five mice over a period of 3 to 8 weeks. The same plane was identified on consecutive days using coarse alignment based on superficial blood vessels followed by careful alignment to reference images at various levels of magnification in the red channel (using tdTomato expression). AAV-mediated expression of GCaMP6m provides high signal-to-noise compared to other methods; however, viral expression is known to increase over months which can lead to compromised signal over time, which is correlated with nuclear localization of the indicator (Chen et al., 2013; Tian et al., 2009). For this reason, imaging was discontinued when fields-of-view contained several cells with GCaMP6 in the nucleus, and all cells with nuclear localization were excluded from analysis (Figure 2.2 i). These methods are in accordance with other long-term imaging studies (Huber et al., 2012). Event rates of all analyzed cells were stable across time along with other properties of the population activity 3.14. Moreover, our ability to model and predict neuronal activity using behavioral features remained consistent throughout the duration of this experiment. For these reasons we have no reason to believe cell health was an issue in this work.

2.2.10 Within-session processing

We implemented custom-written MATLAB software for streamlined motion correction, definition of putative cell bodies, and extraction of fluorescence traces. Following motion correction based on the Lucas-Kanade method (Greenberg & Kerr, 2009), putative cell bodies were first identified by eye and then binary masks were calculated based on the correlation of fluorescence timeseries between pairs of pixels located within $60\ \mu\text{m}$ of one another in the neighborhood of the identified cell. A continuous-valued, eigenvector-based approximation of the normalized cuts objective (Shi & Malik, 2000) was applied to the pixel correlation matrix, followed by discrete segmentation using k-means clustering. A separate neuropil mask was identified to accompany each cell body, defined using the same normalized cuts and segmentation method. Neuropil contamination was removed from the cell fluorescence time series by subtracting the background time series scaled by a contamination factor. The contamination factor was calculated by regressing the cell fluorescence against the background time series (Figure 2.2 a-f). ROI selection and neuropil subtraction were manually verified and manipulated when necessary using an interface tool that allowed examination of anatomical information and fluorescence traces corresponding to each cluster. The event rate was estimated using a previously described autoregressive deconvolution algorithm (Vogelstein et al., 2010) to minimize the impact of indicator kinetics. This metric describes the relative firing rate of each neuron over time but cannot be used to confidentially identify single spikes. We therefore refer to deconvolved traces as an

estimated event rate.

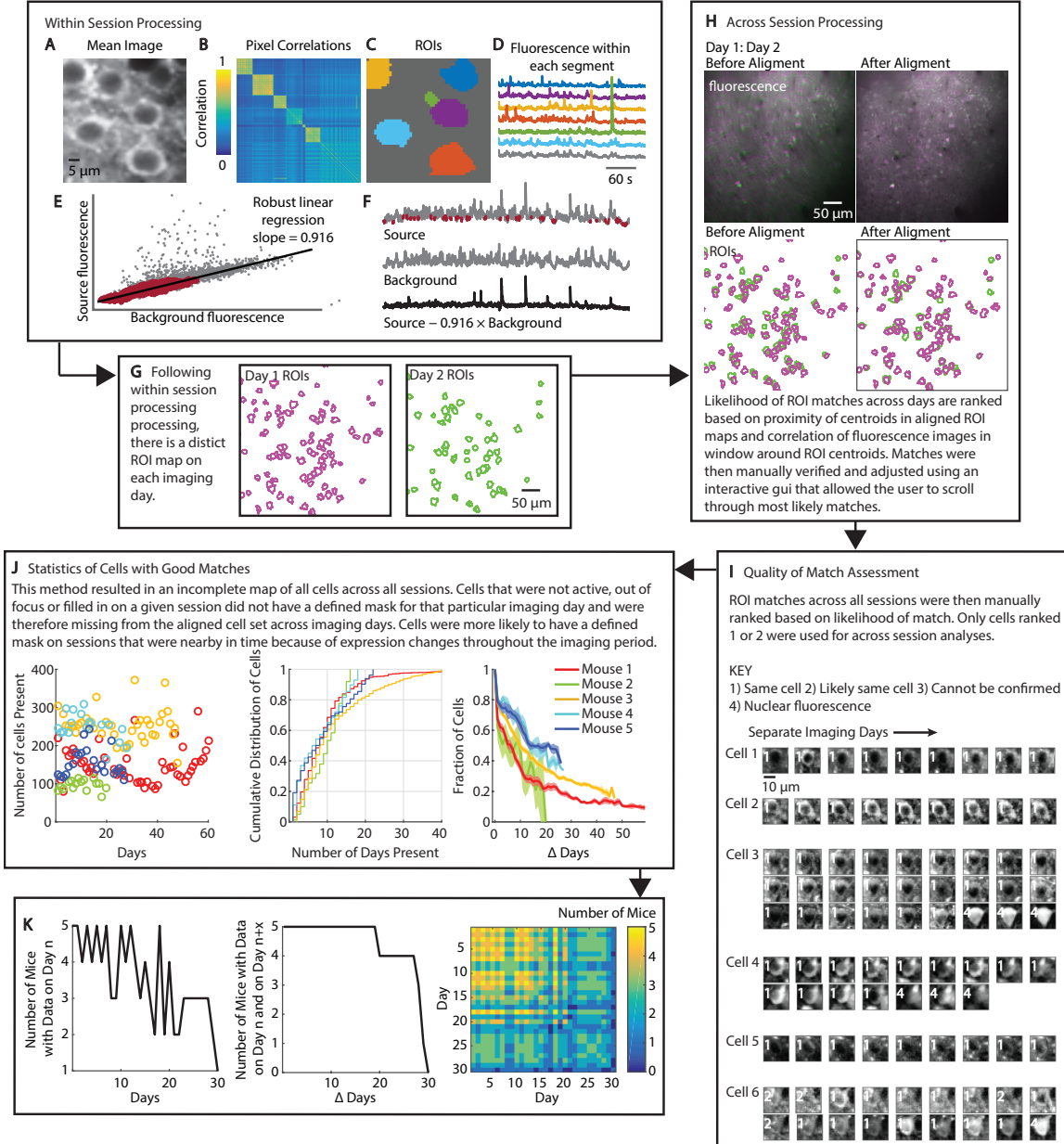
2.2.11 Across-session processing

Binary masks for all fluorescence sources were identified on each day separately and then aligned across days using a semi-automated custom tool. The algorithm ranked cells across imaging days with their most likely matches based on proximity after alignment and anatomical image correlation (a $60 \mu\text{m}$ box around the centroid of the cell). Matches were then verified by eye. This method has advantages over other commonly used approaches. Other approaches often use a single map of ROI masks for all days, such that this map is transformed on each day to best fit that day's imaging alignment. Slight deviations in the axial plane of the image or other sources of in-plane distortion could lead to slight offsets in masks from day-to-day relative to the ideal mask. Such slight offsets could result in contamination from activity in other cells, dendrites, and axons. Our approach identifies signal sources on each day and thus avoids any potential contamination from other signal sources. We then align the signal sources identified on each day to those from other days. The only error that could result is in incorrectly calling two signal sources as the same across days. However, to prevent such errors we visually compared the anatomical images to make sure the signal sources appeared to correspond to the same cell. If a cell could not be confidently identified on a given day, the data were excluded on that day. As a result, our approach resulted in an incomplete map of all cells across all days. We note that cells had to have some activity (calcium transients) in order to be identified on a given day. This activity requirement for the identification of each cell

could potentially result in an underestimation in the extent to which cells gain and lose task related activity. Cells were more likely to have a defined mask on days that were nearby in time due to variable activity and viral expression of the indicator GCaMP6m (Figure 2.2 j).

Figure 2.2 (following page) | Cell identification protocol across days and number of samples for various day comparisons. **a**, Fluorescence image of a $60 \mu\text{m}$ neighborhood of cells. **b**, Correlation matrix between the time series of pixel values within the $60 \mu\text{m}$ neighborhood. **c**, Segmentation of pixels within $60 \mu\text{m}$ neighborhood. **d**, Mean fluorescence time series of pixels within each segment. **e**, ROI fluorescence is regressed against background fluorescence. A neuropil contamination factor is the slope of the best fit line using bottom 8th percentile of ROI fluorescence (red). **f**, Top: ROI fluorescence, bottom 8th percentile labelled in red. Middle: Neuropil fluorescence. Bottom: ROI fluorescence with (contamination factor * background) subtracted. **g**, ROI maps found using protocol in panels **a-f** from two example imaging days. **h**, Top: Overlay of average fluorescence signal from the example imaging days before and after registration based on intensity of tdTomato expression. Bottom: ROI outlines found using protocol in panels **a-f** before and after image registration using the transform from fluorescence image alignment. **i**, Six example cells across all imaging days with identified matches. **j**, Left: Number of cells with good matches identified on each imaging day for each mouse. Middle: Cumulative distribution of number of imaging days with good matches for all cells in each mouse. Right: Probability that a cell was identified with a good match on two days separated by various intervals. **k**, Left: Number of mice with data on each imaging day. Middle: Number of mice with data on two days separated by various intervals. Right: Number of mice with data for each day comparison.

Figure 2.2 | (Continued)



Chapter 3

Dynamic reorganization of neuronal activity patterns in parietal cortex

Laura N. Driscoll, Noah L. Pettit, Selmaan N. Chettih, Matthias Minderer, and Christopher D. Harvey

This and the following chapters are a modified version of a submitted manuscript.

3.1 Introduction

Here we monitored cortical representations of learned associations between arbitrary stimulus-action pairings after these associations had been learned to expert levels. We developed methods to track the activity of populations of neurons and behavioral patterns across weeks as mice performed a navigation-based decision task in virtual reality at near-perfect levels. We focused on activity in the posterior parietal cortex (PPC), which is essential for performing the task and in rodents is considered to function in learned sensorimotor associations, including during navigation (Harvey et al., 2012; McNaughton et al., 1994; Nitz, 2006; Whitlock et al., 2012). We found that activity patterns changed

greatly over the course of days and weeks, such that the population of neurons that provided the most task-relevant information drifted over time. Despite single cell changes over time, the PPC population maintained a steady state with the same statistics of population activity across weeks, such as, for example, a consistent distribution of the fraction of neurons active at each point in the trial. Information about the task could be decoded stably across time using a readout of population activity despite changes in individual neurons, and representations of newly learned cue-response relationships could be incorporated without perturbing existing representations. Our results reveal that single cell representations for learned associations are not stable across long time periods; rather, stability in neuronal representations is maintained at the population level. We propose that drift in neuronal activity patterns could be important for mediating a tradeoff between stable encoding of information and flexibility for incorporating new information.

3.2 Results

We trained mice to perform a navigation based two-alternative forced-choice task. Mice navigated through a T-maze in visual virtual reality (Harvey et al., 2012) (Figure 3.1 a). Mice saw one of two possible visual cues (white walls or black walls) throughout the first half of the T-stem. Mice then ran through a delay period in the second half of the T-stem in which the walls were identical between trial types. At the T-intersection, mice had to report a choice about the cue identity by making a left or right turn for a condensed milk reward. Mice learned this task over 4-6 weeks of training and reached expert behavioral

performance that was mostly stable over weeks (Figure 3.1 b).

3.2.1 Tracking behavior and neuronal activity over weeks

During the task, we imaged the activity of hundreds of layer 2/3 PPC neurons simultaneously using volumetric two-photon calcium imaging. Imaging locations were identified based on stereotaxic coordinates, and separate experiments revealed that these coordinates corresponded to a location anterior to cortical regions identified using retinotopic mapping (Figure 2.1). Here we call this region PPC and note that recent work from the Allen Brain Institute calls this region VisA (?) and that this region is medial to what previous work has called secondary visual area A (Wang & Burkhalter, 2007) (Methods 2.1.7). Imaging sessions were performed typically every day with occasional one-day gaps between sessions (Figure 2.2). On each day we identified the same field-of-view so that we could track activity patterns of neurons across time (Figure 3.1 c-d). We developed a conservative approach to ensure as best as possible that we identified the same neurons across imaging days. First, we identified fluorescence signal sources (putative cells) on each day independently. Signal sources were selected on the basis of temporally correlated fluctuations between pixels, rather than using manual, anatomical selection methods that can fail to separate nearby cells, dendrites, and axons (Hamel et al., 2015; Peron et al., 2015b). Second, to match putative cells across all imaging days, we used a custom algorithm based on distance between regions-of-interest (ROIs) and similarities in the fluorescence images surrounding each ROI. Finally, we visually compared each identified cell across all days to ensure that each cell appeared

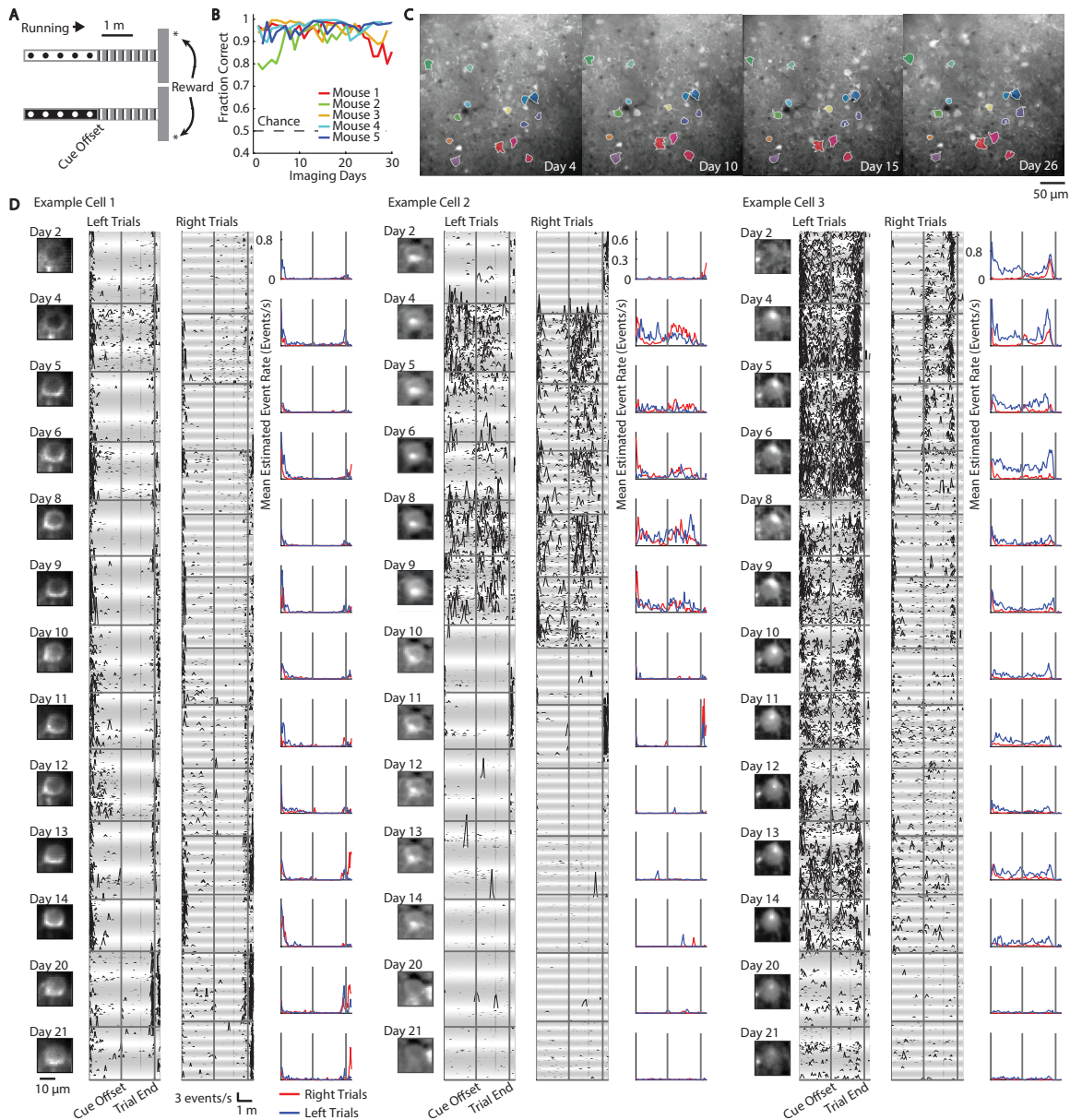


Figure 3.1 | Chronic imaging during stable performance of a virtual-navigation decision task. **a**, Schematic of the two trial types based on a virtual T-maze. Patterns indicate those presented on the virtual maze walls. **b**, Behavioral performance on individual imaging days for each mouse. **c**, Example images of GCaMP6m-expressing neurons across days. One of four imaging planes from volumetric imaging is shown. Some examples of cells identified across days are colored. **d**, The activity of three example cells over three weeks. Left columns: mean GCaMP6m fluorescence image. Middle columns: deconvolved fluorescence signal on individual correct white cue-left turn and black cue-right turn trials. Right columns: mean activity on correct white cue-left turn (blue) and black cue-right turn (red) trials. See Methods 2.2 for cell identification protocol across days.

consistent in the anatomical images and had highly similar ROIs assigned to it (Figure 2.2). We only considered cells on days in which they were identified; other days, in which we could not with high confidence identify the cell, were excluded from our analysis, such that not every cell was identified on every day. This approach was aimed to minimize mislabeling of neurons across days and was intended to be conservative compared to previously developed methods (Huber et al., 2012; Liberti et al., 2016; Peron et al., 2015b; Peters et al., 2014; Poort et al., 2015; Ziv et al., 2013) (see Figure 2.2 and Methods 2.2.11 for a full discussion).

3.2.2 Necessity of PPC activity for post-learning performance of the task

The activity patterns of PPC neurons on a single imaging day were consistent with those reported previously (Harvey et al., 2012; Morcos & Harvey, 2016). On each day, individual neurons were transiently active, with different neurons active at different time points, such that PPC activity tiled the entire duration of a trial (Figure 3.2 a). Many of these responses were reliable and selective for a particular trial type. For example, some cells were more active on black cue-right turn trials than on white cue-left turn trials or vice versa.

The activity in the PPC appeared necessary for the mouse to perform the behavioral task. We virally expressed channelrhodopsin-2 in parvalbumin-expressing inhibitory interneurons at a location centered at the PPC and activated these neurons to inhibit excitatory activity on a subset of trials. Inactivation of PPC decreased the behavioral performance of the mouse from 85 % correct to just above chance levels (Figure 3.2 c). These results were obtained

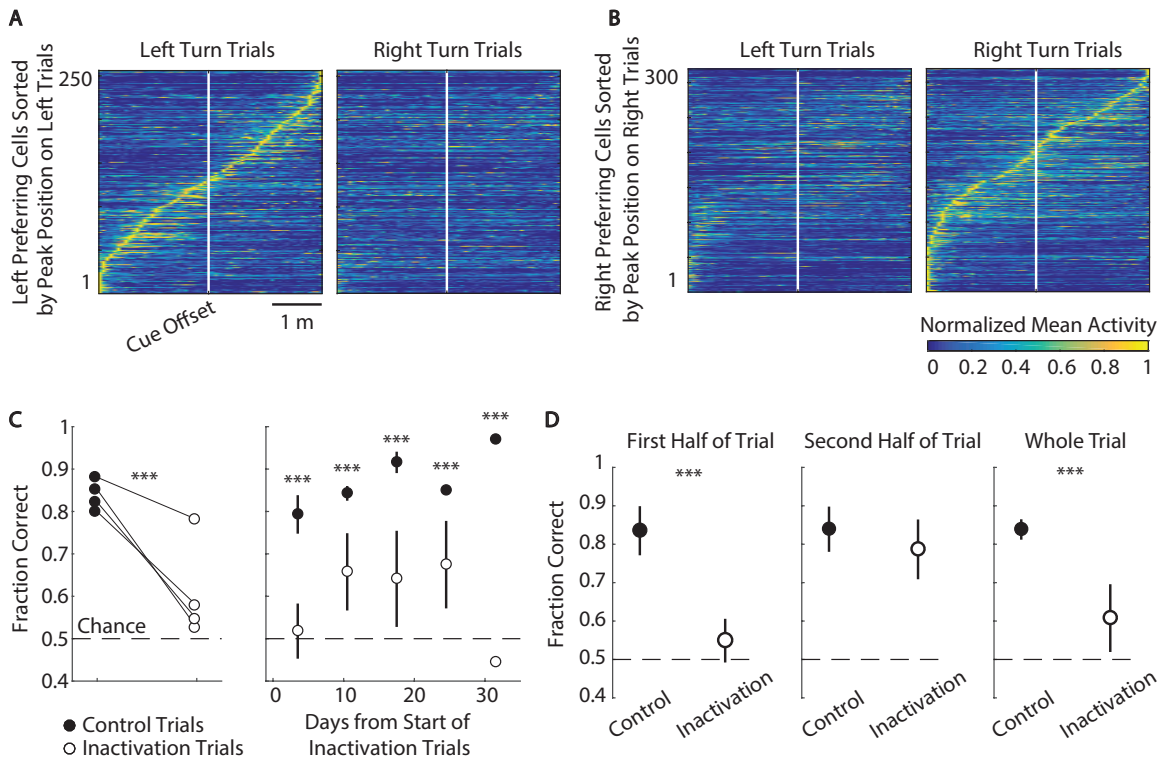


Figure 3.2 | Neuronal population dynamics and inactivation experiments. **a-b**, Mean activity of neurons with a significant peak of activity on **a** left turn trials and **b** right turn trials (Methods 3.6.2) from 5 mice. Traces were normalized to the peak of each cell's mean activity on preferred trials from a single day and sorted by the peak position. **c**, Left: Task performance on optogenetic PPC inactivation and control trials for 4 mice. Trials were combined across multiple days. No significant effect was observed for a control mouse not expressing ChR2: $p = 0.18$. Right: Task performance for inactivation and control trials within non-overlapping 7 day time bins. Error bars indicate mean \pm sem for $n=3,3,4,2,1$ mice for each of the time bins, respectively. *** indicates $p < 0.001$ between control and inactivation trials (bootstrap analysis with shuffled trial labels). **d**, Optogenetic inactivation during the first half of the T-stem (left), second half of the T-stem (middle), and entire T-stem (right). For each manipulation, trials were pooled across multiple sessions. Points indicate mean \pm sem. $n=4$ mice. *** indicates $p < 0.001$ based on bootstrap shuffle of control and inactivation trial labels. $p = 0.06$ for the second half of the T-stem (middle).

days or weeks after the mouse achieved plateau behavioral performance, suggesting that PPC activity was necessary for performing the task even in the post-learning phase. These results were in agreement with earlier work that used pharmacological methods to inactivate the PPC and other studies showing a role for the rodent PPC in visual decision tasks (Goard et al., 2016; Harvey et al., 2012; Licata et al., 2016; Raposo et al., 2014). To further resolve the role of PPC in this task, we then inhibited PPC activity at different segments, either during the first half of the trial or the second half of the trial. Interestingly, we found that when PPC activity was inhibited in the first half of the trial, the mouse's performance was greatly impaired (Figure 3.2 d). In contrast, inhibiting PPC activity during the second half of the trial had no significant effect ($p = 0.06$) on the mouse's performance (Figure 3.2 d). This result is consistent with what has been reported previously in other tasks (Goard et al., 2016; Licata et al., 2016; Raposo et al., 2014). We note that it is difficult to interpret what this finding means in terms of PPC's role in the task: PPC activity could be involved in the transformation of the sensory information into a behavioral action plan or in some aspect of visual processing or potentially other computations. We also note that although inactivation was centered on PPC, such activity manipulations may not be isolated solely to PPC, as has been shown in other systems (Otchy et al., 2015).

3.2.3 Reorganization of sequential activity across maze locations

To compare the activity patterns of neurons across days, we first focused on sequential activity throughout a trial. On each day, a sequence of neuronal activity was present (Figure 3.3 a), top left, center, and bottom right panels). To determine whether this sequence of

activity was the same from day to day, we sorted neurons based on where in the maze they had a reliable peak of activity. We then used the same sorting to look for the same sequence of activity on earlier or later days. Strikingly, the sequence of activity that was present on one day was largely different on other days (Figure 3.3 a). Cells that had a significant peak of activity in the maze on a given day were unlikely to have a significant peak of activity at the same or nearby position after long intervals (Figure 3.3 b). Over time this likelihood of a consistent peak position approached levels expected from a random reorganization of neuronal identities (Figure 3.3 b). These changes resulted from cells with a peak of activity on one day either losing that peak of activity or having a shift in the peak location on subsequent days, both of which increased in likelihood as a function of time from when a peak was identified (Figure 3.3 d). In some cases, peaks shifted by distances larger than one meter. The loss of peaks of activity was offset by an approximately constant rate at which cells initially lacking a peak of activity gained an activity peak (Figure 3.3 d), resulting in a consistent fraction of active cells with significant peaks over the imaging period of weeks ($22.0 \pm 0.5\%$ of neurons, mean \pm sem) (Figure 3.3 c). Together these results indicate that the same activity patterns were not repeated for long time periods.

3.2.4 Different populations of neurons with trial type-specific activity patterns

across days

We also investigated changes in activity patterns that could be related to information about the trial type. Specifically, we asked if the neurons that had different activity patterns on trials with different cues and choices, and thus provided information potentially useful for

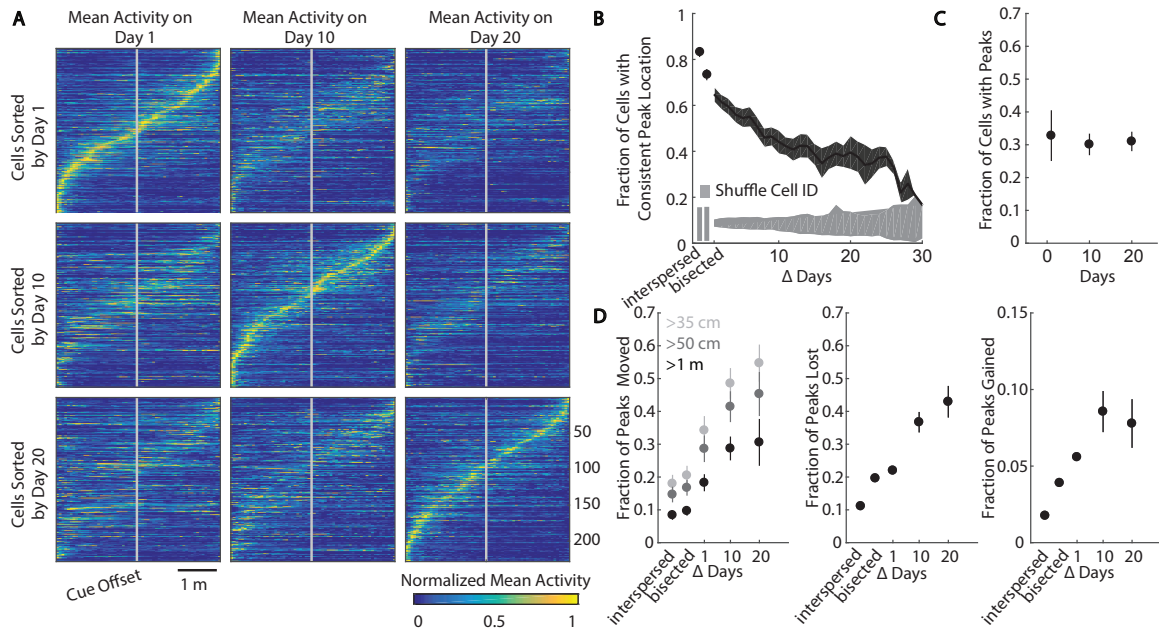


Figure 3.3 | Reorganization of activity within a trial across days. **a**, Normalized mean activity of neurons that were identified on all three imaging days (1, 10 and 20) and that had a statistically significant peak in the sorted day (95 % confidence). Sorting was the same for each day within a row and was different across rows. Gray lines indicate cue offset. **b**, For all cells with a highly significant (99 % confidence) peak of activity on a given day, the fraction of cells that had a significant(95 % confidence) peak of activity at a similar location (< 70 cm shift) on a subsequent day. Shading indicates mean \pm sem ($n = 5$ mice; some large interval data points had fewer than 5 mice, see Figure 2.2. The gray shaded area indicates 95 % confidence intervals of chance levels based on shuffling the cell IDs separately on each day. Fraction of cells with consistent peak location vs. time: $p < 10^{-8}$, ANOVA. Interspersed and bisected groups correspond to comparisons across half of data within a given session that was either interspersed throughout the session, or divided into first and second halves. **c**, Fraction of cells that had a significant peak on the noted day. Fraction vs. time: $p = 0.85$, ANOVA. In panels c-d, error bars indicate mean \pm sem, $n = 5,5,4$ mice for the time intervals shown. **d**, Left: For cells with a significant peak on day n and day n+x, the fraction of peaks that shifted by greater than 35 cm, 50 cm and 1 m. Fraction moved 35 cm vs. time: $p = 0.019$, ANOVA. Center: For cells with a highly significant peak on day n, the fraction of cells that did not have a significant peak on day n+x. Fraction lost vs. time: $p < 10^{-9}$, ANOVA. Right: For cells without a significant peak of activity on day n, the fraction of cells that had a highly significant peak on day n+x. Fraction gained vs. time: $p = 0.96$ ANOVA. Interspersed and bisected groups correspond to comparisons across half of data within a given session that was either interspersed throughout the session, or divided into first and second halves.

solving the task, were the same across time. For each neuron on each day, we used a decoder to quantify how well that neuron's activity across the entire duration of a single trial could predict the trial type (white cue-left turn vs. black cue-right turn, correct trials only). On a given day, a significant fraction of active neurons had a decoding accuracy above chance ($29.1 \pm 1.1\%$ of neurons, mean \pm sem, with $p < 0.05$ compared to decoding with shuffled trial labels). Neurons that had high decoding accuracies on a given day, and thus different activity patterns between trial types, did not necessarily have significant decoding accuracies on subsequent days (Figure 3.4 a-b). The large majority of neurons that were identified on more than 15 imaging days only had above chance decoding accuracy on less than half of those days (Figure 3.4 c). Moreover, only 1.6% of these neurons had significant decoding accuracy on all days in which they were identified. The likelihood that a cell with greater than chance decoding accuracy on a given day also had significant decoding accuracy on a subsequent day decreased with the interval between compared days (Figure 3.4 d). Over time the likelihood that a cell maintained significant decoding accuracy decreased to levels approaching those consistent with a random reorganization of cell identities (Figure 3.4 d). We tracked the subpopulation of neurons that was the most highly informative about trial type on a given day. Over time, the distribution of decoding accuracy within this subpopulation approached and largely overlapped with the distribution of the entire population, indicating that this subpopulation was not a special set of highly selective neurons across all time points (Figure 3.4 e).

We also examined if the neurons with selective activity for one trial type (e.g. black cue-

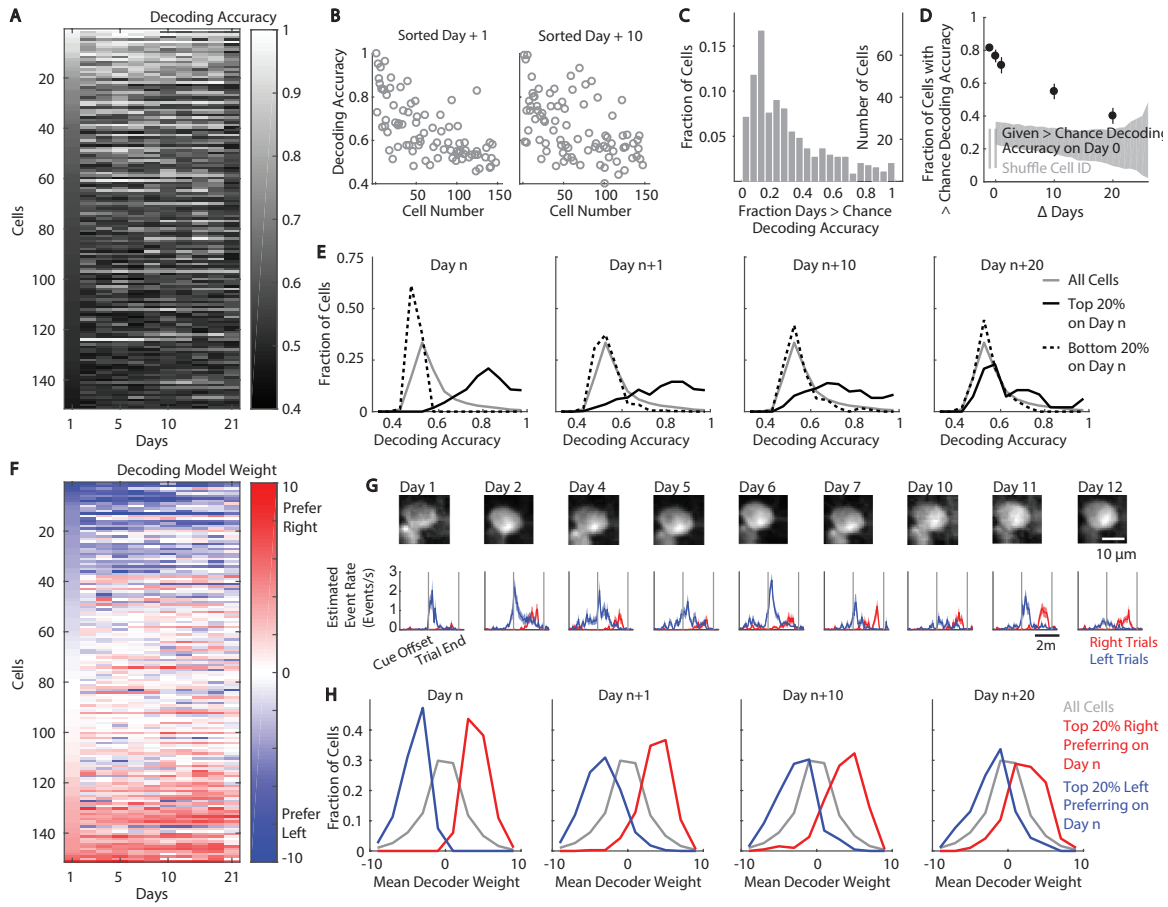


Figure 3.4 | Reorganization of information about trial-type across days **a**, Decoding accuracy for trial type based on the activity of individual neurons, sorted by decoding accuracy on Day 1. **b**, For an example day, cells were sorted by their trial-type decoding accuracy. Decoding accuracy is shown for a held out set of data on the day used for sorting (black) and on subsequent days (gray). **c**, For the cells that were identified on ≥ 15 days, the fraction of days in which a cell's activity provided above chance decoding accuracy, relative to the number of days in which the cell was identified. Chance was determined as $p < 0.05$ (bootstrap analysis with shuffled trial labels). **d**, Given high confidence for significant decoding accuracy on day n (real data performed better than 990 of 1000 shuffles), the fraction of cells with greater than chance decoding accuracy (real data performed better than 950 of 1000 shuffles) on day $n+x$. Interspersed and half groups indicate fraction of cells with consistent decoding accuracy across odd/even trials and first/second half of trials respectively. Error bars indicate mean \pm sem $n = 5$ mice. The gray shaded area indicates 95 % confidence intervals of chance levels based on shuffling the cell IDs separately on each day. Fraction of cells that maintain significant decoding accuracy vs. time: $p < 10^{-11}$, ANOVA. **e**, On a given day, the cells with the top 20 % and bottom 20 % of decoding accuracies were identified. The distributions of decoding accuracy for these cells are shown in comparison to the distribution for all cells after intervals of 1, 10, and 20 days. **f**, Trial type preference for the cells in panel A sorted by trial type preference on day 1. Model weights with positive values indicated higher activity on black cue-right turn trials. A model weight was determined at each spatial bin in the maze, and the mean weight was calculated for each cell. **g**, Example of a single cell with dynamic trial-type information. Top: mean fluorescence image of the cell body. Bottom: mean activity of the cell on correct white cue-left turn (blue) and black cue-right turn (red) trials. **h**, On a given day, the cells with the top 20 % largest weights for white cue-left turn and black cue-right turn trials were identified. The distributions of trial-type weights are shown in comparison to the distribution for all cells after intervals of 1, 10, and 20 days.

right turn trials) switched to having a preference for the other trial type (e.g. white cue-left turn trials) (Figure 3.4 f-h). The most highly selective cells for each trial type over time often lost their selectivity or gained additional selectivity, at other points in the maze, for the other trial type (Figure 3.4 f-g). We tracked the neurons that had the strongest preferences for each trial type on a given day (Figure 3.4 h). Over days, the trial type preferences of these neurons approached that of the entire population. Only a small fraction of neurons switched from having statistically significantly higher activity on one trial type to having statistically significantly higher activity on the opposite trial type ($4.7 \pm 1.7\%$ of cells, mean \pm sem; lower bound for chance: $1.4 \pm 0.7\%$ based on switches within a day using a hold out set; upper bound for chance: 45 - 50% based on switches in selectivity when cell IDs were shuffled across days). Switches in trial type preferences were thus rare from one day to the next, and gains or losses of selectivity were more common. Together these results indicate that the population of neurons that had trial type-specific information was largely different across days, with larger differences in these populations over longer time windows.

3.2.5 Using a generalized linear model to compare relationships between neuronal activity and behavioral features across days

These findings together provide evidence that major changes and reorganization of neuronal activity patterns occurred during stable performance of a behavioral task. However, these analyses only considered two aspects of the task (position in the maze and trial type) and did not include other task features that could potentially be represented in the neuronal activity. For example, PPC has been considered to be important for

movement planning and could thus have activity related to the running patterns of the mouse (Andersen & Cui, 2009; Nitz, 2006; Whitlock et al., 2012). In addition, PPC receives inputs from visual areas and might have activity related to the movement of visual stimuli projected on the screen, such as during turning compared to forward motion (Harvey et al., 2012; Oh et al., 2014). We wanted to understand whether behavioral variability across days could explain the changes in neuronal activity or alternatively if these changes were due primarily to single neurons having different relationships between their activity and the behavior of the mouse across time. We therefore developed an approach to describe an individual neuron's activity on single days based on a large number of variables that described the task and mouse's behavior. We developed a generalized linear model (GLM) in which we modeled the activity of an individual neuron based on the running patterns of the mouse on the spherical treadmill, the virtual maze position (visual scene), the trial type, reward events, and whether the mouse was in the inter-trial interval period (Friedman et al., 2010; Park et al., 2014) (Figure 3.5 and Figure 3.6).

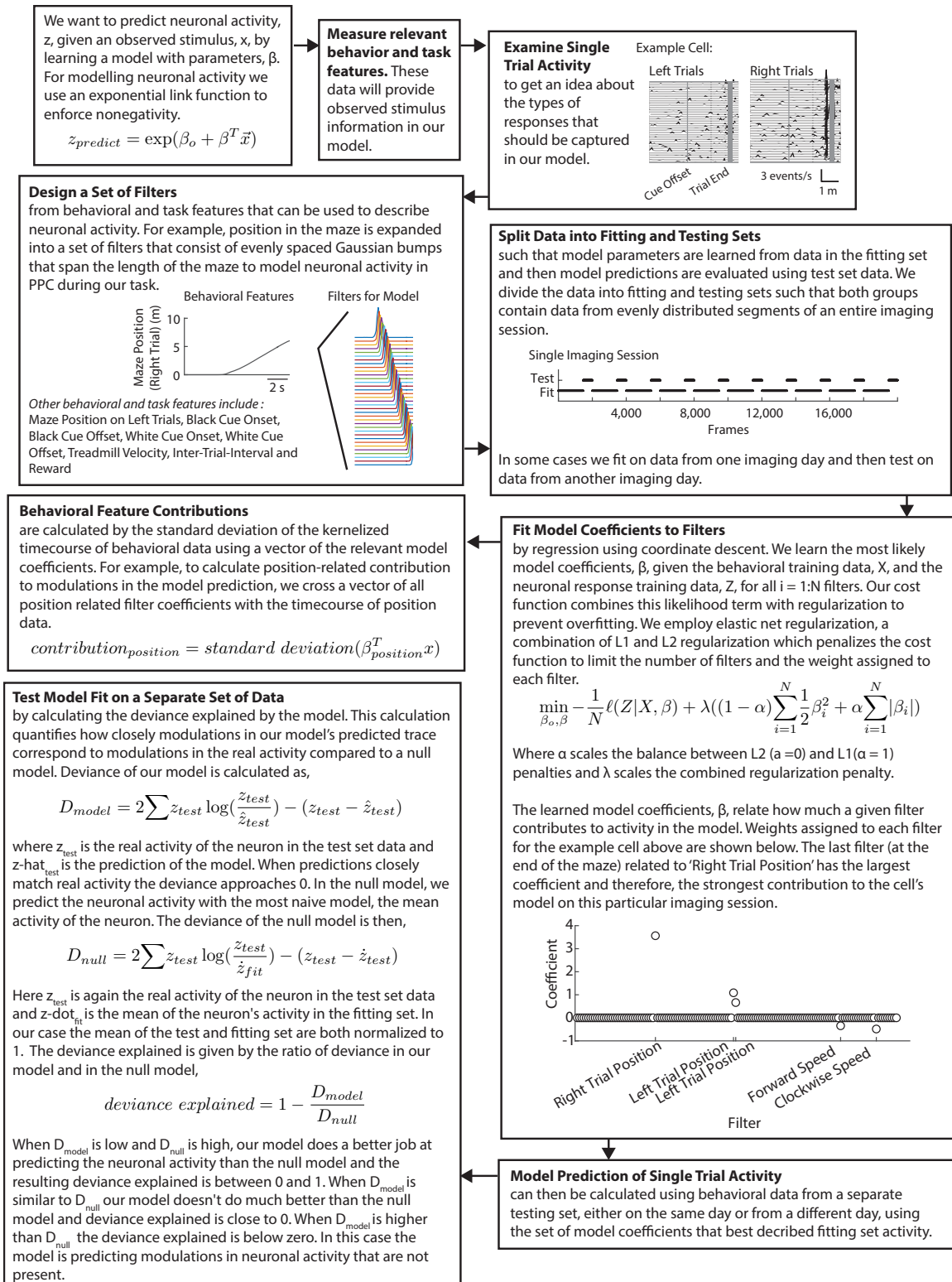
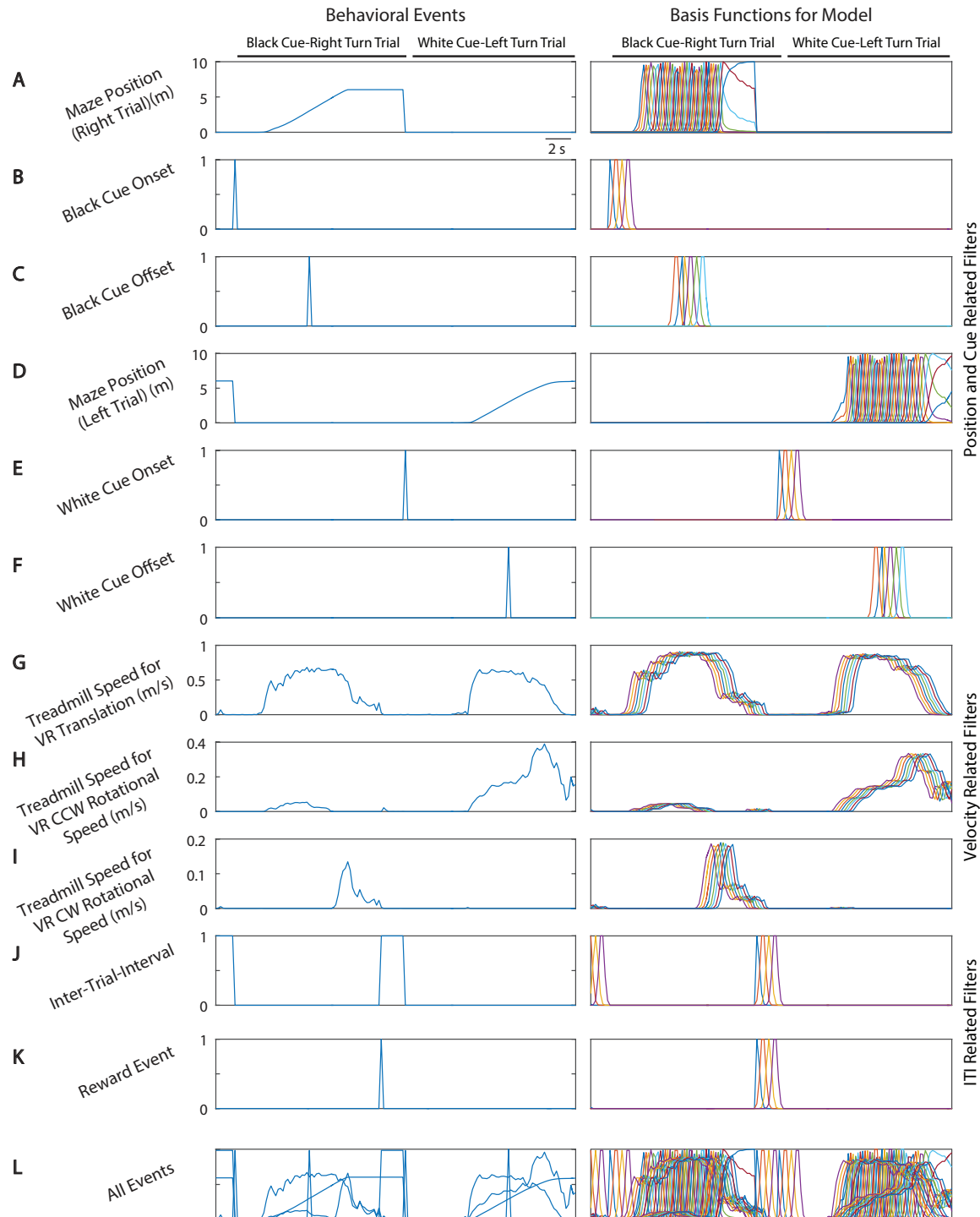


Figure 3.5 | GLM fitting procedure

Figure 3.6 (following page) | Basis functions for encoding model. Trial and behavioral measurements during each imaging frame (left) were expanded into a set of basis functions that were incorporated into the GLM (right). Filter groupings used in contribution calculation for Figure ?? shown in right margin. **a**, Left: Maze position on right turn trials. Right: 36 spatial boxcar filters of position spanning the length of the maze were convolved with a Gaussian filter for right turn trials. **b**, Left: Black cue onset. Right: 4 Gaussian basis functions that span the first 2 seconds of black cue-right turn trials. **c**, Left: Black cue offset (delay period onset). Right: 6 total basis functions, 2 basis functions extended for 1 second preceding cue offset and 4 basis functions extended for 2 seconds following cue offset. **d**, Left: Maze position on left turn trials. Right: 36 spatial boxcar filters of position spanning the length of the maze were convolved with a Gaussian filter for left turn trials. **e**, Left: White cue onset. Right: 4 Gaussian basis functions that span the first 2 seconds of white cue-left turn trials. **f**, Left: White cue offset (delay period onset). Right: 6 total basis functions, 2 basis functions extended for 1 second preceding cue offset and 4 basis functions extended for 2 seconds following cue offset. **g-i**, Left: Movement of spherical treadmill. Right: 8 basis functions total for each of 3 running speed signals were extended 1 second forward and backward in time to model predictive and responsive signals. **j**, Left: Inter-trial interval Right: 4 basis functions that extended for 2 seconds forward in time following trial end. **k**, Left: Inter-trial interval Right: 4 basis functions that extended for 2 seconds forward in time following reward. **l**, Left: All trial and behavioral measurements. Right: All basis function for GLM, excluding novel cue onset and offset (same as black and white cue basis functions).

Figure 3.6 | (Continued)



We fit the relationship between a cell's activity and these behavior and task features to develop a model of that cell's activity-behavior relationship. We tested the quality of this model by predicting the cell's activity based on the behavioral and task features in a subset of trials not used for fitting. If the predicted activity closely matched the real activity, we concluded that our model could describe the activity-behavior relationship for the cell on that day. Across cells, models were able to explain a large fraction of neuronal activity ($57.9 \pm 2.6\%$ of cells, mean \pm sem, had significant fits measured as the explained deviance in the neuronal activity compared to a null model) (Figure 3.7 c). We fit separate models for each neuron on each day. The distribution of model prediction qualities for each day across the population was consistent throughout the duration of our several week study (Figure 3.7 d).

We used these models to compare the relationship between a cell's activity and behavioral features across days. Using the model of a cell's activity-behavior relationship fit on a single day, we predicted the cell's activity based on behavior features in other days (Figure 3.8). If the model developed on one day was able to predict activity on a subsequent day, then we concluded that a consistent activity-behavior relationship existed. In contrast, if a model developed on one day failed to predict the activity on subsequent days, then we concluded that a consistent activity-behavior relationship was absent. This approach has the potential to track stable relationships between neuronal activity and behavior features across days that traditional approaches might miss. For example, if a neuron had activity related to the running patterns of a mouse and if these running patterns changed relative to position in the maze across days, the GLM could potentially reveal a

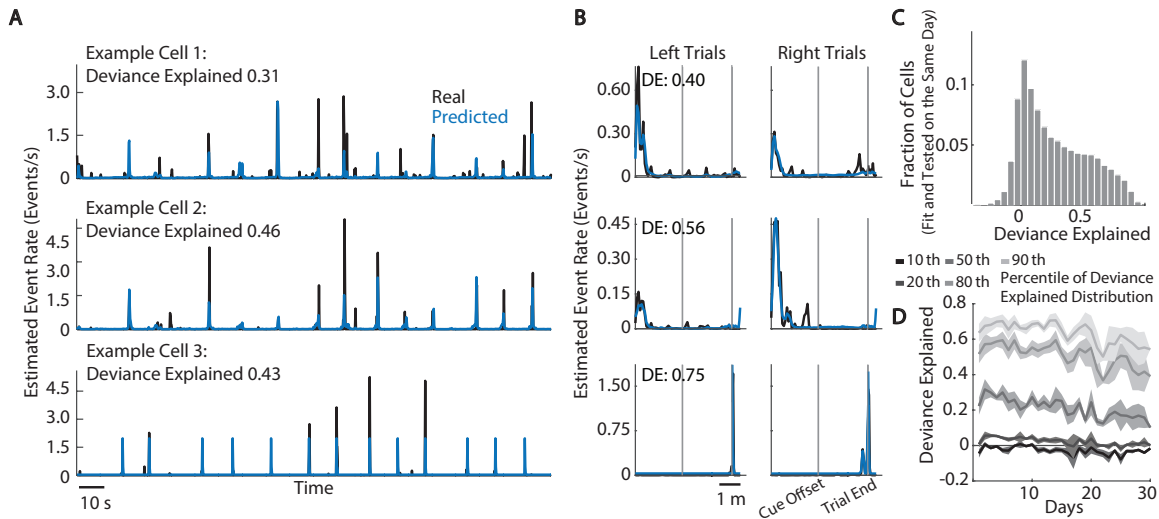


Figure 3.7 | Fitting activity-behavior relationships with a generalized linear model. **a**, For three example cells, a segment of activity is shown (black) along with the activity predicted from the GLM (blue). Deviance explained is calculated directly from single frame predictions. **b**, Same as in panel A, except for the mean activity on white cue-left turn and black cue-right turn trials. Deviance explained is calculated from trial averaged predictions, concatenated white cue-left turn and black cue-right turn mean activity. **c**, Distribution of the quality of model fits measured by deviance explained compared to a null model for trial averaged predictions (Methods 3.6.3.3). The model was fit and tested on data from the same day. $n = 17,353$ model fits across cells and days. **d**, Distribution of deviance explained for models fit on each day divided into five groups. Similar distributions of fits were apparent on each day. Shaded regions indicate mean \pm sem for $n = 5$ mice (fewer mice on some later days, see Figure 2.2 j for the number of mice at each interval).

stable activity-behavior relationship over time that would be missed if only maze position were analyzed. Importantly, behavioral features, such as running speed and trial duration, were variable across trials, but maintained a similar distribution and range of values on each day, suggesting that models should be transferable across days (Figure 3.9). We limited effects due to fitting procedures, such as regularization, and due to correlated task variables by fitting and testing bidirectionally for each pair of days (see Methods 3.6.3.3 for a full discussion).

3.2.6 Changing activity-behavior relationships in single neurons over days

Models of activity-behavior relationships developed on a given day were, on average, able to predict activity patterns well on neighboring days, but did a poor job of predicting activity patterns as the time between the compared days increased (Figure 3.8 c). Over long intervals, model predictions eventually reached that of a null model (for intervals greater than 17 days), indicating that a cell's activity-behavior relationship was generally inconsistent over weeks (Figure 3.8 c). We also quantified similarity of models for a given cell across days using Kendall rank correlations of model parameters and found a comparable decay over time (Figure 3.10).

The changes in these activity-behavior relationships were made up of cells that lost well-modeled relationships, gained well-modeled relationships, and switched relationships across days. To quantify the prevalence of these events, we used a statistical threshold, based on shuffled data, to binarize model performance into models that

A Single Neuron Encoding Model Fit and Tested on Different Days

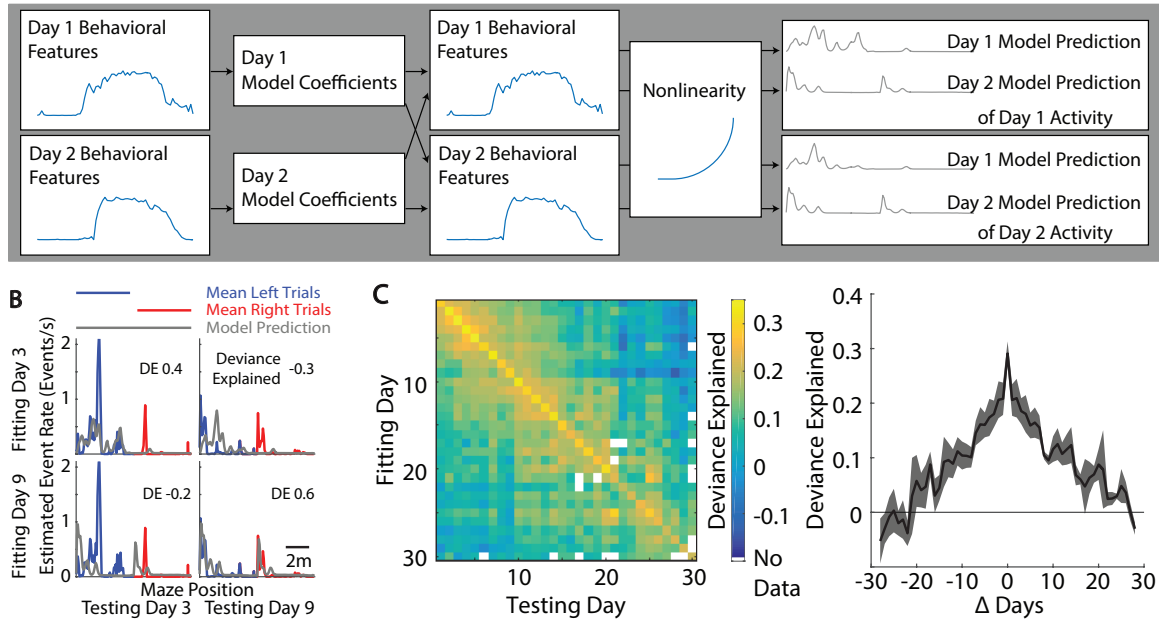


Figure 3.8 | Fitting activity-behavior relationships with a generalized linear model. a, For each neuron on each day, a separate generalized linear model was fit to the activity of the neuron based on behavior and task features. Each day's model was then tested for how well it could predict activity-behavior relationships on other days. Model coefficients for behavioral filters were fit on one day and then applied to behavioral data from another day to produce a prediction of the neuronal activity time course for that day. **b,** For an example cell, mean activity for white cue-left turn (blue) and black cue-right turn (red) trials on imaging days 3 and 9. One model was fitted on data from day 3 and another model was fitted on data from day 9. Each model was used to make a prediction (gray) about the neuron's activity based on behavioral data in a test set, either from the same day or the other day. The model fit quality was quantified as the deviance explained. **c,** Left: Deviance explained by models fit on a one day and tested on the same or a different day. Values were averaged across all cells for each mouse and then averaged across mice. Each entry has a variable number of data points (and in some case no data points, white values) due to varying durations of imaging periods for mice and gaps between imaging days (Figure 2.2 k). Right: Average deviance explained as a function of time between the fitting and testing days. Shading indicates mean \pm sem.

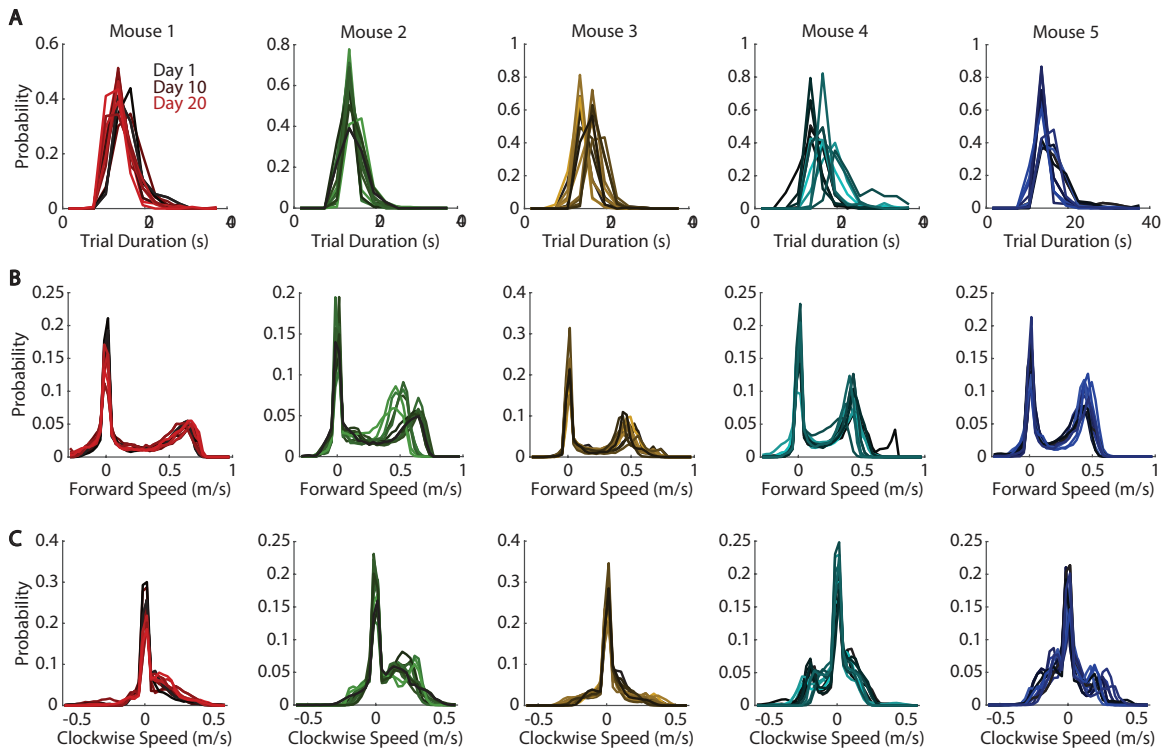


Figure 3.9 | Behavioral features were variable but had overlapping distributions across days **a**, For each mouse, the distribution of trial durations from cue onset to trial end. **b**, For each mouse, the distribution of treadmill speed for forward translation in the virtual environment (about the pitch axis relative to the mouse's body axis). **c**, For each mouse, the distribution of treadmill speed for rotation in the virtual environment (about the roll axis relative to the mouse's body).

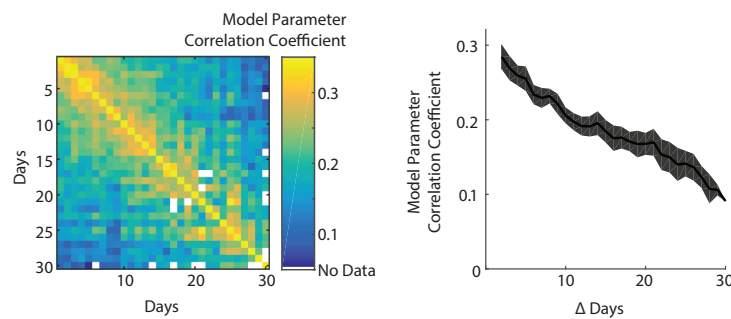


Figure 3.10 | Model comparison across days. Left: Kendall rank correlation coefficients of model beta coefficients fit on separate days. Diagonal values are 1. The values were averaged across all cells for each mouse and then averaged across mice. Each entry has a variable number of data points (and in some case no data points, white values) due to varying durations of imaging periods for mice and gaps between imaging sessions. See Figure 2.2 j for the number of mice at each interval. Right: Average correlation coefficient when fit and tested on data separated by n days. Shading indicates mean \pm sem.

predicted activity patterns above chance levels (significant predictions) and models that provided poor predictions of activity (Methods 3.6.3.3). We then compared pairs of models fit on separate days for a given cell. If the models developed on one day provided good predictions of the activity patterns on the other day, then the cell was considered to have a consistent activity-behavior relationship (Figure 3.11 a). Instead, if one model with a significant prediction of activity could be developed for one day's activity but not for the other day's activity, then the cell was considered to have lost or gained an activity-behavior relationship (Figure 3.11 a). If models with significant predictions could be developed on both days but these models provided poor predictions of activity on the other day, then the cell was considered to have switched activity-behavior relationships (Figure 3.11 a). The likelihood that a cell lacking an activity-behavior relationship gained such a relationship remained constant throughout the imaging period of weeks ($26.8 \pm 0.01\%$ of cells) (Figure 3.11 c). As the time interval between the compared days increased, the likelihood that a cell had a consistent relationship decreased, and the likelihood that a cell lost or switched a relationship increased (Figure 3.11 c). After 20 days, a cell that had a well-described activity-behavior relationship was more likely to have lost this relationship or switched to a different relationship than to have maintained its original relationship (Figure 3.11 c). This rate of change was consistent throughout the entire imaging period. The likelihood that a cell gained, lost, switched or maintained an activity-behavior relationship from one day to the next remained constant throughout the imaging period of weeks. (Figure 3.11 d)

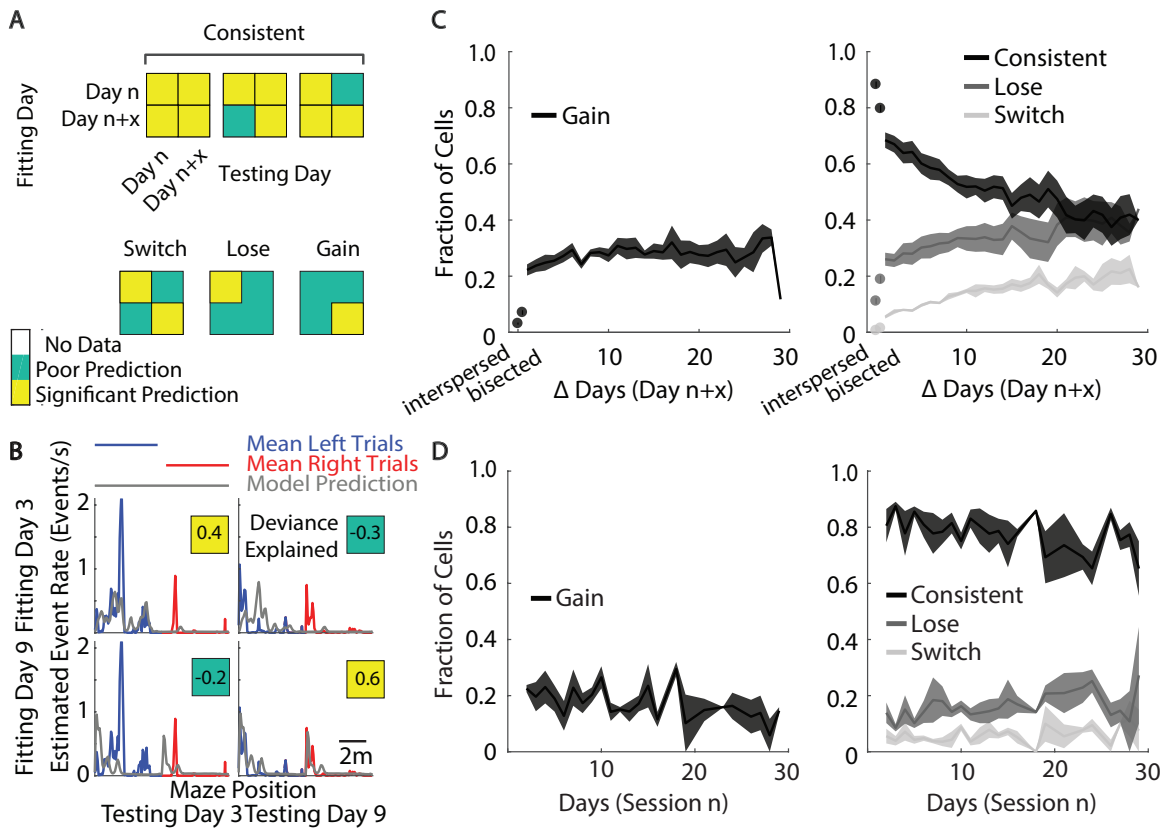


Figure 3.11 | Quantification of consistent, lost and gained activity-behavior relationships. **a**, Schematic for model comparisons binarized as significant and poor predictions using a statistical threshold of 0.2 deviance explained. This threshold was chosen based on fits from a bootstrap analysis in which behavior data were circularly shifted relative to neuronal activity (Methods 3.6.3.3). Separate models were fit to an individual cell's activity on two days and tested on the fitted day or on the other day (as in Figure 3.8 c). **b**, For an example cell, mean activity for white cue-left turn (blue) and black cue-right turn (red) trials on imaging days 3 and 9. One model was fitted on data from day 3 and another model was fitted on data from day 9. Each model was used to make a prediction (gray) about the neuron's activity based on behavioral data in a test set, either from the same day or the other day. The model fit quality was quantified as the deviance explained, which was thresholded and labelled as a 'poor prediction' or a 'significant prediction' (Methods 3.6.3.3). **c**, Left: For cells without a significant model prediction on day n, the fraction of cells that had a significant model prediction after a given interval. Right: For cells with a significant model prediction on day n, the fraction of cells with consistent (black), lost (medium gray), or switched (light gray) activity-behavior relationships after a given interval. Shaded area indicates mean \pm sem ($n = 5$ mice; some large interval data points had fewer than 5 mice, see Figure 2.2). Interspersed and bisected groups refer to models that were trained and tested on half of the data from a single session and compared to the corresponding model, trained and tested on the opposite half of the data from the same session. The interspersed group compares models that were built from interspersed chunks throughout the duration of the session and provides a baseline for change due to measurement noise. The bisected group compares models that were built from the first and second half of the session. **d**, Left: For cells in which a model with a significant prediction of activity could not be developed on day n, the fraction of cells that had a model with a significant prediction of activity that could be developed on day n+1. Shaded region indicates mean \pm sem across mice $n = 5$ (fewer mice on some later days). Right: For cells with a significant model prediction on day n, the fraction of cells that had consistent (black), lost (medium gray), and switched (light gray) activity-behavior relationships on day n+1. Shaded region indicates mean \pm sem. $n = 5$ (fewer mice on some later days).

The rates at which neurons had changes in their activity-behavior relationships varied greatly across cells (Figure 3.12 a). For each neuron, we calculated the likelihood that a model developed on one day provided a significant prediction of another day's activity (Figure 3.12 b, left) and fit an exponential to this likelihood over time to define a metric of consistency for each cell (Figure 3.12 b, right). Some neurons had slow decays and thus had relatively consistent activity-behavior relationships, whereas others had fast decays indicative of rapid changes. Over a 20 day interval, the large majority of neurons had a low likelihood of consistent models (Figure 3.12 c). Only 7.3% of neurons had consistent activity-behavior relationships over the entire interval (defined as > 95% significant predictions after 10-20 days). To understand if the neurons with the most and least consistent activity-behavior relationships represented different types of behavioral information, we examined the contribution of various parameters to each cell's activity (the extent to which the behavioral parameter of interest modulated a given cell's model prediction, see Methods 3.6.3.5). Cells with the most consistent and least consistent relationships had a distribution of contributions for trial type, position in the maze, running pattern, and inter-trial interval activity that overlapped with the distribution in the full population (Figure 3.12 d). However, neurons with the least consistent relationships more often had greater contributions from trial type and maze position than neurons with the most consistent relationships (Figure 3.12 d). Our results therefore suggest that there was a continuous distribution of stability in activity-behavior relationships across neurons, with activity related to learned task features (trial type and maze position) possibly having

less consistency across time.

The changes in activity-behavior relationships did not reflect independent relationships across days. Rather, consistent relationships in the recent past were predictive of consistent relationships in the short-term future. Neurons with a consistent activity-behavior relationship for two or more consecutive days prior to a particular imaging day were more likely to maintain that relationship than neurons which had a consistent relationship for only one of the immediately preceding imaging days (Figure 3.12 e). These results suggest that neurons potentially operated with modes of activity that tended to persist for neighboring days such that a neuron's activity on each day was not independent of the recent history of its activity. However, the predictive power of recent consistency fell off after ten days, suggesting there was not a separate population of permanently consistent cells (Figure 3.12 e).

The GLM analyses therefore suggest that the changes in activity we observed were likely due to unstable activity-behavior relationships, rather than changes in behavioral patterns across days. We further supported this finding by comparing the similarity of population activity patterns on trials with the most similar or least similar behavioral patterns across all days. The population activity was more similar on those trials with more similar behavioral features, measured as correlations between population activity vectors (Figure 3.13 a). However, the difference in activity similarity between the most and least similar behavioral trials was small compared to the population activity changes across time (Figure 3.13 a). In addition, we did not observe any evidence that the mouse forgot and

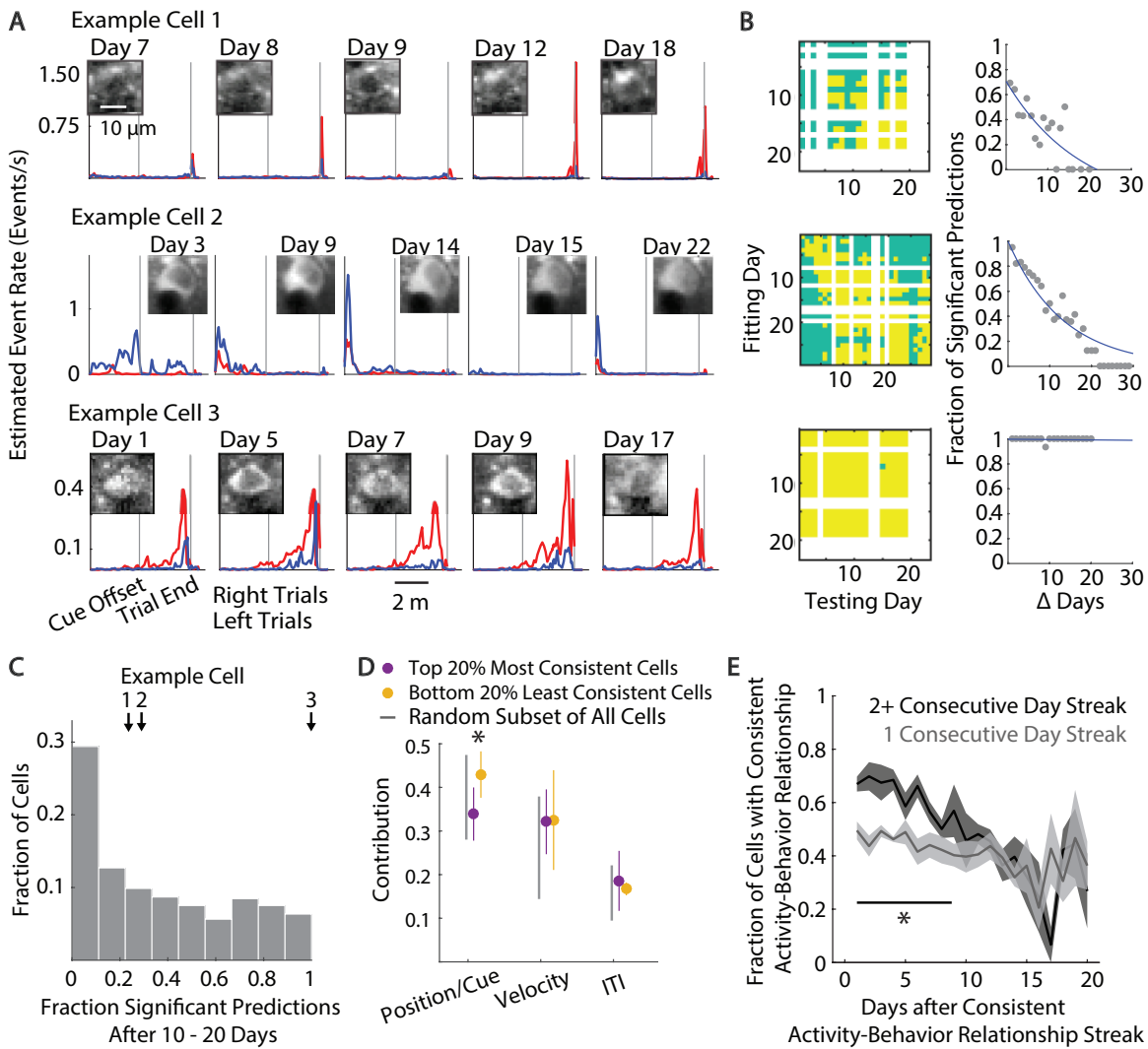


Figure 3.12 | Distribution in the rate of change across cells in the population. **a**, Mean activity for three example cells with varying consistency in activity-behavior relationships. **b**, Left: For example cells from panel f, matrix of fitting and testing comparisons as in panel . Right: Fraction of models with significant predictions as a function of time between the fitting and test days. Exponential fits are shown, weighted by the number of model comparisons that went into each data point. **c**, Histogram of the fraction of significant model predictions after 10-20 days of separation between the fitting and training days for all cells identified in at least 15 imaging days. $n = 690$ cells.

d, Contribution of different categories of behavior/task features to neuronal activity, estimated as the standard deviation of the linear part of the model (Methods 3.6.3.5). For comparisons of cells with the 20 % most and 20 % least consistent models : Position/cue, $p = 0.026$; treadmill velocity, $p = 0.98$; whether the mouse was in the inter-trial interval, $p = 0.79$; t-test. Error bars indicate mean \pm sem. $n = 5$ mice. Grey lines indicate 95 % confidence intervals for 20 % of randomly selected cells. **e**, On a given day, we identified for how many previous days the model of that day's activity provided a good prediction of previous day's activity. Models with significant predictions for data on ≥ 2 consecutive previous days were more likely to provide a good prediction in future days than models with significant predictions for data on only 1 previous day. * indicates $p < 0.05$, t-test.

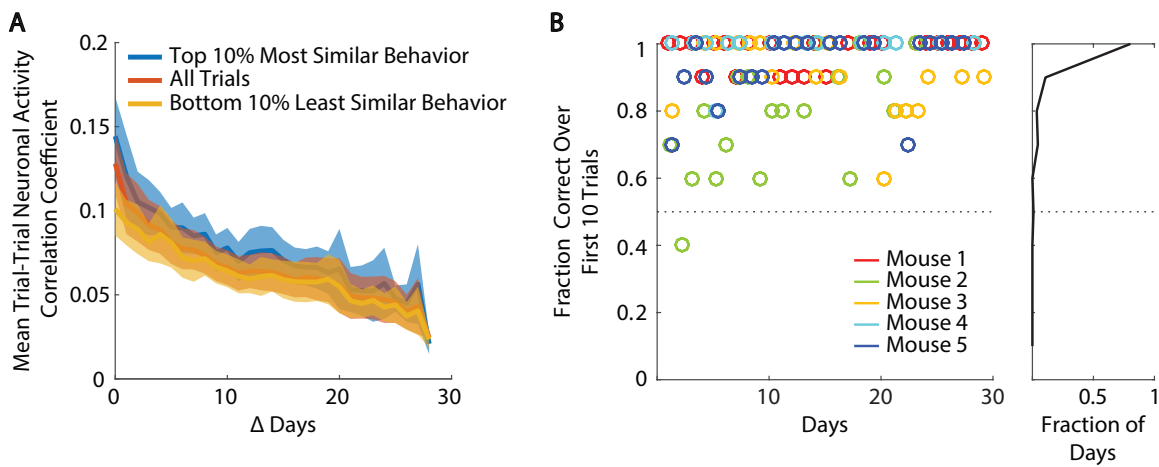


Figure 3.13 | Behavioral change across days does not explain neuronal change. **a**, Similarity in population activity as a function of days separating sessions for the trials with the most or least similar behavioral patterns. Behavioral patterns were compared using a mean vector of all measured behavioral parameters (forward speed, clockwise speed, view angle, position along stem axis, and position along arm axis) at each position in the maze (5 parameters \times 21 spatial bins). Similarity was determined as the pairwise trial-trial correlation coefficient of this behavioral parameter vector. Population activity patterns were compared using a vector of population activity (neurons \times 21 spatial bins). Similarity was determined as the pairwise trial-trial correlation coefficient of this population activity vector. Trials with more similar behavioral patterns were often found on sessions that were separated by a smaller time interval. However, there were some pairs of sessions in the top 10 % most similar that spanned the full duration of our experiment, and some pairs of sessions in the 10 % least similar that were found in neighboring days. **b**, Left: Behavioral performance over the first ten trials on each imaging day for all mice. Right: Cumulative density plot of behavioral performance on the first ten trials of imaging days.

re-learned the task on each day because mice performed at near perfect levels, even on the first few trials of each day (Figure 3.1 b, Figure 3.13 b).

3.2.7 Consistent statistical features of population activity on each day

Despite these changes in the activity of individual neurons, we noticed that consistent patterns were present in the population activity on each day. As shown above, neuronal activity that tiled the full trial duration was present on each day and was made up of different neurons across days (Figure 3.3). The distribution of population activity across the trial was not uniform, but this distribution was highly similar across all days in a given population of neurons (Figure 3.14 a-b). In addition, on each day, a decoder for trial type

based on population activity achieved similar levels of performance and had similar distributions of performance across time points in the trial (Figure 3.14 c-d). Interestingly, in each population of neurons from different mice, differences between mice were maintained across days. For example, the population of neurons in one mouse (red) had higher decoding accuracy of trial type than did the population of neurons in another mouse (green) across all days (Figure 3.14 d). These differences were maintained with a similar shape across the duration of the trial (Figure 3.14 c). Many other properties of population activity had similar distributions on each day, including for neuron-neuron activity correlations (Figure 3.14 e-f), trial-trial population activity correlations (Figure 3.14 g-h), estimated population firing rates (Figure 3.14 i-j), and decoding accuracy of trial type for individual neurons (Figure 3.14 k-l). These results indicate that even though properties of activity in individual neurons changed across time, the statistical features of population activity were largely consistent over weeks. Therefore, the population appeared to have a 'set point' of similar activity each day, using different neurons, and neurons in different ways, to achieve this steady state.

3.2.8 Decoding of information from dynamic neuronal representations

The changes in neuronal activity-behavior relationships over time raise questions about how information could be read out from such a dynamic neuronal population over days and weeks. One possibility is that the cells with the most consistent activity-behavior relationships are those that preferentially carry information for the readout. Alternatively, it could be possible that the activity in the cells with less consistent activity-behavior

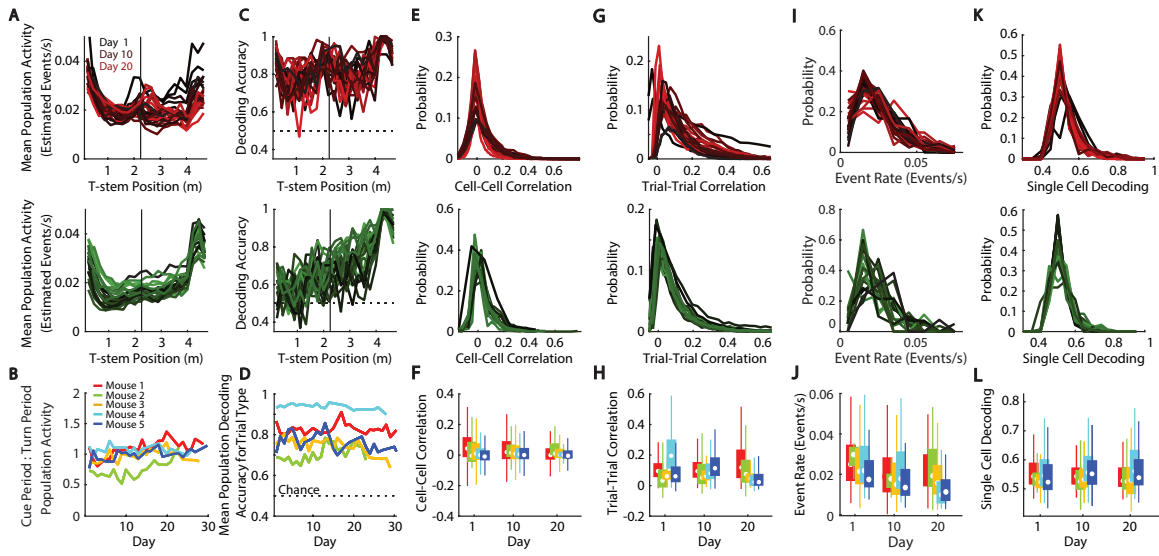


Figure 3.14 | Stable statistical features of population activity. **a**, For two example mice, the mean population activity as a function of position in the maze. Darker to lighter colors indicate earlier to later days. **b**, Ratio of activity in the cue period to the delay period on each day for each mouse. **c**, For two example mice, population decoding accuracy of trial type as a function of position in the maze. Separate decoders were trained at each spatial bin and on each day. **d**, Population decoding accuracy of trial type for each mouse on each day. **e**, For two example mice, distributions of cell-cell correlations of deconvolved calcium signals smoothed with a 2-second sliding window across all pairs of neurons on each day. **f**, Summary of cell-cell correlation distributions for all mice for days 1, 10 and 20. Boxes represent the 25th and 75th percentiles, white dots indicate the mean, and whiskers show the 99 % range of the data. **g-l**, Same as in panels e-f, except for correlations of the matrix of population activity (cells x maze position) between trials of the same type **g-h**, activity event rates in the population of neurons estimated from deconvolved calcium signals **i-j**, and classification accuracy of trial type based on single-cell activity patterns **k-l**.

relationships also allows decoding of information over time. We investigated this issue by testing various decoding strategies for reading out the trial type on the basis of population activity.

We first trained and tested a linear decoder on each day separately using all neurons (as in Figure 3.14 c-d). We found trial type information could be decoded throughout the duration of the trial, with higher decoding accuracies at the end of the trial, when the mouse executed a turn at the T-intersection (Figure 3.15 a). We then compared the decoding performance using the cells with the most consistent activity-behavior relationships and the least consistent relationships, defined by exponential fits of model performance decay over time (from Figure 3.8 b, see Methods 3.6.3.3). The population of cells with the least consistent activity-behavior relationships had better decoding accuracy throughout the majority of the trial than did the cells with the most consistent relationships. In the final segment of the trial, when the mouse executed a turn, decoding accuracies were similar between groups (Figure 3.15 b).

To analyze the stability of information in activity patterns, we tested decoding performance across days. We trained a decoder on a given day and tested it on subsequent days (Figure 3.15 c). When considering a random subset of cells, decoding performance decreased as the interval between compared days increased. This result was present throughout the duration of the trial (Figure 3.15 c). In the cells with the most consistent activity-behavior relationships, decoding performance was low and consistent across time for the majority of the trial (Figure 3.15 c, left and middle). For the final segment of the

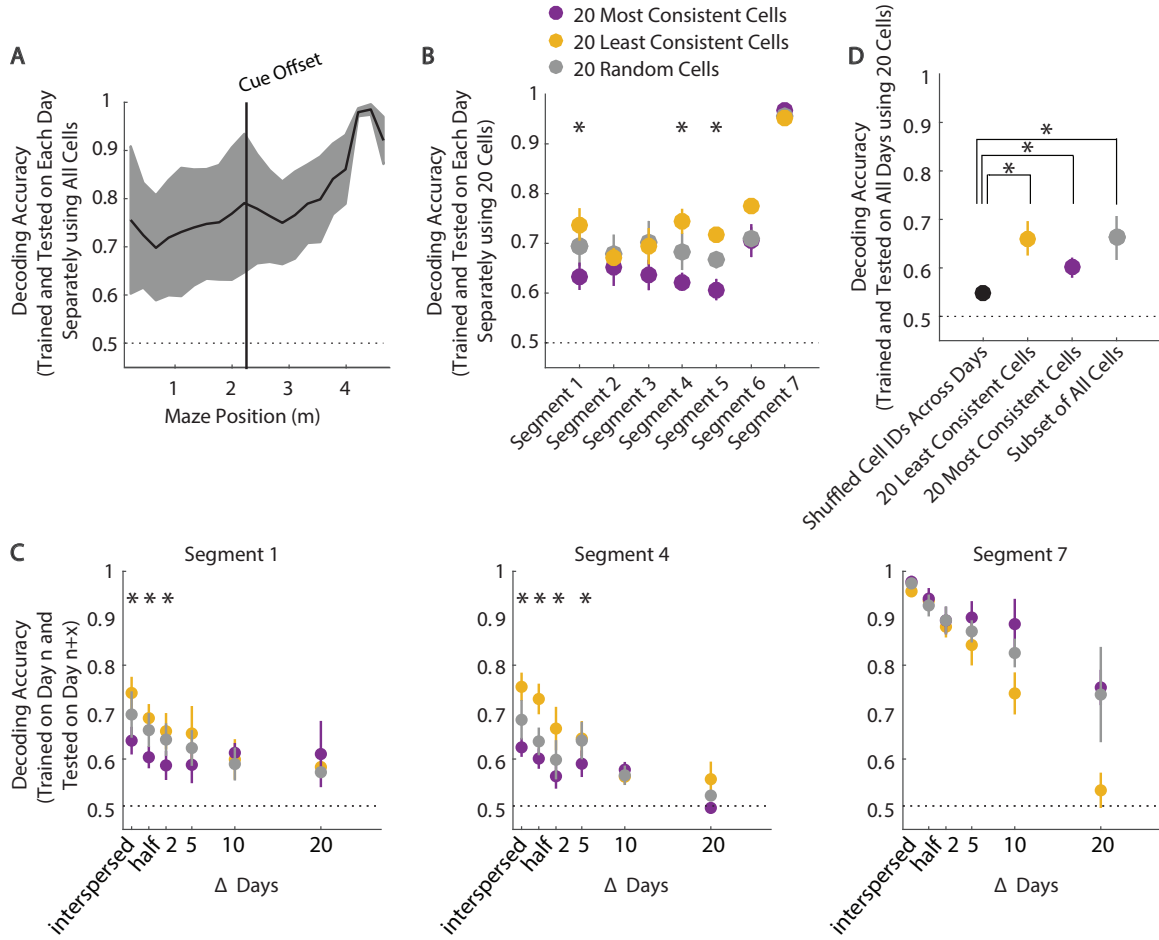


Figure 3.15 | Decoding task information across days. **a**, Population decoding accuracy of trial type on correct trials as a function of position in the maze. The decoder was trained and tested on the same day. Separate classifiers were trained at each spatial bin and on each day. Shaded region indicates mean \pm sem. $n = 5$ mice. **b**, Population decoding accuracy of trial type on correct trials using 20 cells with the least consistent activity-behavior relationships (yellow), 20 cells with the most consistent activity-behavior relationships (purple), and 20 randomly selected cells (gray) for 7 segments of the trial, which included 3 spatial bins each. The decoder was trained and tested on the same day. Error bars indicate mean \pm sem. $n = 5$ mice. * indicates $p < 0.05$, t-test, between least consistent and most consistent groups. **c**, Decoding performance when the decoder was trained on a given session and tested on a later session for segment one (left) segment four (middle) and segment seven (right). Error bars indicate mean \pm sem. $n = 5, 5, 4, 4, 2$ mice for Δ days 0, 2, 5, 10, 20 respectively. * indicates $p < 0.05$, t-test, between least consistent and most consistent groups. Interspersed and bisected groups refer to population decoders trained on odd/even trials and tested on even/odd trials or trained on the first/second half and tested on the second/first half of a single session respectively. **d**, Decoding performance when the decoder was trained on data from all days and tested on a separate set of data from all days. In addition to the conditions from panel **b** and **c**, decoding was performed with cell IDs shuffled separately for each individual day (cells did not have a consistent ID across days). Error bars indicate mean \pm sem. $n = 5, 5, 4, 4, 2$ mice for Δ days 0, 2, 5, 10, 20 respectively. * indicates $p < 0.05$, t-test, between shuffled cell IDs and the indicated other group.

trial, the decoding performance in these cells was high and consistent over days (Figure 3.15 c, right). As expected, the performance of a decoder trained on one day and tested on other days decreased as a function of time for the cells with the least consistent activity-behavior relationships (Figure 3.15 c). Interestingly, however, over intervals within one week, these cells performed better in the majority of the trial than the cells with the most consistent relationships (Figure 3.15 c, left and middle). Together, these results indicate that the information in the population was not stable over time, but some information remained in the population for days and weeks, even in neurons with the least consistent activity patterns.

If the relevant information for the task must be read out near the time the mouse executes a turn, then it might be beneficial to weight strongly the activity of the cells with the most consistent activity-behavior relationships. In contrast, if information in the T-stem is more relevant for behavior, then weighting the activity of the cells with the less consistent relationships might be beneficial. Our cue and delay period inactivation experiments demonstrate that PPC is required during the cue period only, when the least consistent cells had more information about trial type. Therefore, it is possible that the task-relevant information in the cells with the least consistent activity-behavior relationships could be of importance for PPC's role in this task.

These results suggest that to maintain high levels of information across time, an ideal readout would need to change in a coordinated manner with the encoding network. However, we wanted to test if it might be possible to identify a stable readout in the form

of a single decision plane that could be used across all days to separate trials of different types on every day. We combined all imaging days together and trained a decoder on a subset of trials and tested this single decision boundary on other trials that were distributed across all days. We compared the performance of this combined-day decoder using only the neurons with the least consistent activity-behavior relationships, the most consistent relationships, or a random sample of all neurons (Figure 3.15 d). In these cases, the cells with the least consistent relationships provided information at a similar level as the other groups and allowed decoding of trial type above chance levels. When the identities of the cells were shuffled independently on each day, the ability to find a stable readout decreased significantly, indicating that the decoding performance required the structure of the population activity over days (Figure 3.15 d). This analysis therefore reveals that, for the binary classification of trial type over the time intervals examined, it is possible to find a stable readout of population activity that performs above chance levels, even from the most dynamic population of neurons. However, to achieve higher performance, a readout that changes dynamically with the encoding network would likely be necessary.

3.3 Discussion

Our results reveal that during stable performance of a learned navigation task, the activity patterns in PPC were variable over the timescales of days and weeks. These findings indicate that through the course of learning, neuronal activity patterns in PPC did not converge to a single representation. Rather, there appeared to be a set of activity patterns

in the PPC population that were similarly sufficient for the task. Importantly, many statistical features of the population activity were consistent across days, such that the population appeared to reach a set point. However, the PPC neurons that were used in this representation, and how these PPC neurons were used, changed across days.

3.4 Acknowledgements

We thank Ofer Mazor and members of the Harvey lab for comments on the manuscript. We thank Paola Patella and Matthias Minderer for contributing to the design and setup of the inactivation experiments. We also thank the Research Instrumentation Core at Harvard Medical School. This work was supported by a Burroughs-Wellcome Fund Career Award at the Scientific Interface, the Searle Scholars Program, the New York Stem Cell Foundation, the Alfred P. Sloan Research Foundation, a NARSAD Brain and Behavior Research Young Investigator Award, NIH grants from the NIMH BRAINS program (R01MH107620) and NINDS (R01NS089521), an Armenise-Harvard Foundation Junior Faculty Grant, a Edward R. and Anne G. Lefler Center Predoctoral Fellowship and Junior Faculty Award, the Albert J. Ryan Fellowship, and the Stuart H.Q. and Victoria Quan Fellowship. C.D.H. is a New York Stem Cell Foundation Robertson Neuroscience Investigator.

3.5 Author contributions

L.N.D and C.D.H. conceived of the project. N.L.P. designed and performed inactivation experiments and analyzed associated data. M.M. designed retinotopy experiments and

analyses and built the widefield microscope. S.N.C. and M.M. designed cell selection algorithm and gui for extracting single session ROI maps. L.N.D. designed across session alignment algorithm and gui for aligning ROI maps across days. L.N.D and C.D.H designed all other experiments and analyses, and L.N.D. performed these experiments and analyses. L.N.D. and C.D.H. wrote the manuscript.

3.6 Data analysis methods

3.6.1 General analysis procedures

For visualization of mean and single trial activity, activity was spatially binned into 66 segments (60 in the stem and 6 in the arms) followed by 2 seconds (10 imaging frames) during the inter-trial interval. Spatially binned segments typically contained 1 imaging frame each per trial. Data was interpolated to fill in gaps in which a bin contained no imaging frames on a trial. These analyses were only used for fine-resolution measurements of locations of peak activity. For the majority of the analyses (all except Figure 3.3), we binned the data into larger segments (21 segments, 23 cm/bin). Neuronal activity and behavioral parameters were averaged in each bin in this case. Each bin typically contained 2-3 frames/trial. Unless otherwise noted, all analyses were performed on correct trials only. Correlation coefficients were calculated from Pearson's correlations unless otherwise noted.

3.6.2 Identification of significant peaks of activity

Here we used 60 spatial bins during the T-stem rather than 21 spatial bins because we were interested in achieving greater resolution of spatial reorganization. Mean activity across 60 spatial bins were calculated for correct white cue-left turn and black cue-right turn trials. To identify statistically significant peaks of activity, behavior data time courses were circle-shifted by a random amount relative to neuronal activity time courses, and new means were calculated for 1000 random shifts. All locations where the mean activity in the unshifted data was greater than activity in 950 shuffles for three consecutive bins were considered to contain a significant peak of activity. For all analyses where peaks were compared across days, we tracked peaks that were labelled with high confidence (unshifted data was greater than activity in 990 shuffles for three consecutive bins). Peaks were labelled as 'gained' or 'lost' if in the absent session, there was below 95 % significance for a peak at that location. We found this gap between thresholds for the presence or absence of a peak to be important for limiting measurement noise. By these criteria for change, we found peak consistency across odd and even trials within one session to be $83.2 \pm 2.1\%$.

3.6.3 Encoding model

On each day separately, we fit a Poisson Generalized Linear Model (Friedman et al., 2010) to the estimated event rates of each cell based on measured behavioral and task variables. While our estimated event rates were not necessarily Poisson distributed, mean responses scaled with the variance and rates were larger than zero, suggesting that the Poisson model

was appropriate for our data.

3.6.3.1 Model parameters

All measured behavioral and task-related variables were temporally averaged into bins to match the sampling rate of imaging frames. Variables include x and y position in the virtual world, running speed on the pitch and roll axes of the spherical treadmill, visual cue onset and offset locations, reward delivery events and trial end (Figure 3.6). Variables provided input for basis functions that were distributed either in space or in time to produce 144 predictors in total. The maze was divided into 36 spatial boxcar filters and convolved with a Gaussian filter separately for right and left turn trials to make the first 72 filters. The onset of each visual cue contributed 4 basis functions (16 in total for all four cues) that spanned the first 2 seconds of the trial. For cue offset (delay period onset), 2 basis functions extended for 1 second preceding cue offset, and 4 basis functions extended for 2 seconds following cue offset (24 in total for all four cues). Running speed signals were extended 1 second forward and backward in time for translational, clockwise and counterclockwise rotational motion (4 filters forward and 4 filters backward for each of 3 speed signals for a total of 24 filters) to model predictive and responsive signals. Trial-end and reward events each contributed 4 basis functions that extended for 2 seconds forward in time (8 filters total). All temporal filters spanned 1 second, overlapping and evenly distributed within each set.

3.6.3.2 Fitting

We used the `glmnet` package in R to fit GLMs. Each day was divided into 10 evenly distributed chunks (first tenth of session, second tenth of session, and so on) and then sub-divided into 11 numbered pieces within each chunk. All pieces with the same number were then combined into groups 1-11. This resulted in 11 groups that contained data that was evenly distributed across the imaging session (Figure 3.5). Seven of these groups were randomly chosen and used as cross validation folds during fitting, and the other three groups were combined and used to test model predictions (7 groups made up 73 % fitting and 3 groups made up 27 % testing predictions). For some figures, we compare models that were trained on a subset of data from a single session. First we divided data from a single session into halves, either interspersed chunks throughout the duration of the session (interspersed) or simply the first and second half of the session (bisected). We then treated these halves as independent sessions that were divided as we previously describe (73 % fitting and 27 % testing predictions). These models were only used for comparison to the appropriate opposite half within a single session. Parameters were fitted for each cell separately with elastic net regularization consisting of 10 % L2 and 90 % L1 methods. Model fitting was conducted on the Orchestra High Performance Compute Cluster at Harvard Medical School. This shared facility is partially supported by NIH through grant NCRR 1S10RR028832-01.

3.6.3.3 Analysis of model

Deviance explained was used as the metric of model fit. It was calculated by comparing the activity predicted by the model to the actual activity, based on the average real and predicted activity levels on white cue-left and black cue-right turn trials. Deviance explained was calculated based only on data not included in the fitting procedure. It was compared to a null model in which the predicted event rate was 1 (the normalized mean rate of the entire fitting set). We also computed deviance explained using predictions of the full time series of activity for single frames. In this case, the distribution of fits was similar, except lower than for trial-averaged data, as expected. To determine whether a model prediction described test data significantly above chance, we compared the deviance explained to the distribution of deviance explained for models in which, before model fitting, the time series of neuronal activity was circle-shifted relative to the time series of behavior data. We found the upper limit of deviance explained in models that were fit on shuffled data to be 0.2 (for trial-averaged activity). Therefore, we determined models with greater than 0.2 deviance explained on test data to have predictions significantly above chance performance. Cells with activity that could not be significantly predicted by our models could still have behaviorally relevant activity patterns that were simply not described by our set of filters. Therefore, when we refer to cells having gained or lost activity-behavior relationships, we refer specifically to the set of relationships included in our models. By comparing model fits between any two days or between

subsets of data from a single day, we could determine whether a given neuron's activity-behavior relationship was consistent over time, gained or lost a relationship to a behavioral feature, or switched from encoding a particular set of behavioral features to encoding another. If models with significant predictions could be fit on each individual day's data for a given pair of days and if the models also provided significant predictions of the other day's activity, then we called the activity-behavior relationship consistent. If models with significant fits could be fit on each individual day's data for a given pair of days and if the models did not provide significant predictions on the other day, we determined a switch in activity-behavior relationship had occurred. If only one day had a model that could predict the neuron's activity significantly well, then we concluded that a gain or a loss of activity-behavior relationship had occurred. This approach works well when behavioral variables are not highly correlated. However, if behavioral variables are very highly correlated, then it is difficult for the model to determine to which variable weight should be attributed. If variables were highly correlated on one day but not correlated in another day, then incorrect assignments of switches in activity-behavior relationships could emerge. To be conservative and to account for any potential cases in which non-modeled variables were highly correlated with modeled variables (on some days but not others), we did not require symmetry in model performance across days for an activity-behavior relationship to be considered consistent. That is, if a model prediction on day i and day j both had significant predictions of activity and if the model from day i predicted well the activity from day j, but not vice versa, then a consistent

activity-behavior relationship would still be considered to be present. In this case, if behavior variables x and y were highly correlated on day j but not on day i , then the model on day j might incorrectly attribute weights on day j leading to a poor prediction on day i . However, because the variables x and y were not highly correlated on day i , then the model would correctly attribute weights on day i , successfully predicting activity on day j despite having correlated variables x and y on day j . This method would still fail to identify a consistent activity-behavior relationship if the 'real' encoded feature (for example, mental state) was correlated with different filters in the model on each day. These subtle behavioral confounds are difficult to remove completely and should be considered in the interpretation of this work and most other behavioral studies. Through the use of virtual reality we could control the sensory environment and track behavioral metrics with great precision, incorporating these features into our models and thus minimizing the aforementioned concerns.

3.6.3.4 Metric of consistency in activity-behavior relationships

We defined the consistency of activity-behavior relationships for each cell by the likelihood that an encoding model fit on a given day continued to provide significant predictions of the cell's activity for days and weeks. We found the fraction of models that provided a significant prediction of a given cell's activity over each interval between fitting and prediction sets (1-30 days). We then fit an exponential decay, weighting each point by the number of model comparisons available (for example, there were more model comparisons where Δ days = 1 than Δ days = 30). We only included cells that had

significant fits on at least half of days where Δ days = 0 because cells with a low starting point necessarily had slow decays (the fraction of significant model fits was bounded between the y-intercept and zero).

3.6.3.5 Contribution of task and behavioral features to the activity of a cell

To calculate the contribution of each task and behavioral variable to a given model, we computed the standard deviation of the linear part of the model that was related to the behavioral variable of interest (the standard deviation of beta coefficients crossed with relevant behavioral filters of behavioral data). This provided us with the extent to which a behavioral variable modulated the activity of the neuron. For filter groupings in position/cue, velocity and ITI contribution calculation see Figure 3.6.

3.6.4 Decoding

We used C-Support Vector Classification with a linear kernel for all decoders. For some decoders, we considered the activity of single cells (Figure 3.4 and 3.14 k). In these cases, the decoder was trained using data from all 21 spatial bins in the trial. In other cases, in which we wanted to assess the time course of information, we trained decoders on each spatial bin separately using the activity of all neurons or subsets of neurons (Figure 3.14 a and 3.15). When decoders incorporated a smaller number of cells (20 cells each for subgroups in Figure 3.15) we divided the maze into larger bins to account for the fact that each only had trial type information for a small portion of the trial. For decoding analyses, the data were divided into two-thirds for training/validation and one-third for testing. The

regularization weight hyperparameter C was selected using a random search with 10-fold cross validation on a subset of training sets across mice. The specific setting of the hyperparameter did not greatly affect the accuracy of our decoders. The same hyperparameter value ($C = 100$) was used for all data sets. Significant decoding accuracies in Figure 3.4 were determined by bootstrap analysis in which behavioral data were circularly rotated relative to each cell's neuronal activity. Cells in which real data performed better than 950 of 1000 shuffles were determined to have significant decoding accuracy. Using this statistical threshold, it is thus expected that 5 % of cells would have significant decoding accuracy by chance.

Chapter 4

Monitoring neuronal activity over days during learning

4.1 Introduction

Given that changing neuronal activity patterns either cause some instability in information coding or require compensation by a dynamic decoding network, it is important to consider what advantages might arise from these changes. Computational models suggest that an advantage of dynamic neuronal representations could be the flexibility of incorporating new information into the population (Ajemian et al., 2013; Rokni et al., 2007). We therefore tested how existing representations were affected by the learning of a new association. We trained the same mice that had already stably performed the task described above to learn a new association.

4.2 Results

4.2.1 Task design for learning a stimulus-action pair

We introduced a third possible cue (crosshatch pattern) that required a specific turn at the intersection for the mouse to receive a reward (the turn direction was randomly selected for

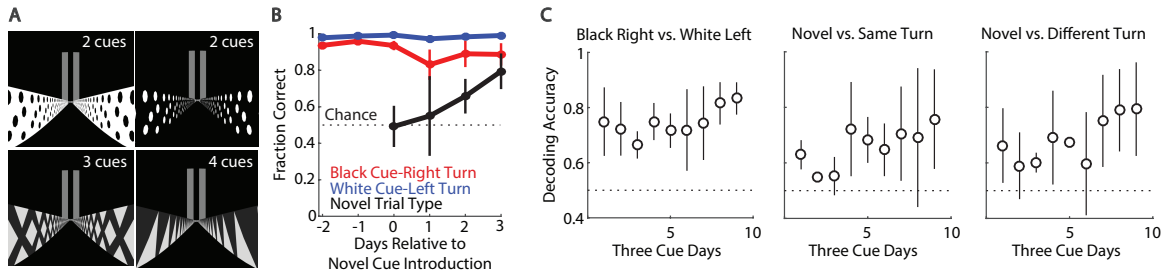


Figure 4.1 | Neuronal activity during learning of a novel trial type **a**, Schematic of virtual maze trial types. **b**, Behavioral performance on 2 days preceding and 4 days following introduction of a novel trial type. Error bars indicate mean \pm sem. $n = 4$ (2 mice with 2 novel trial types each). **c**, Decoding performance of different trial types during the first 1 second of the cue period based on population activity. Error bars indicate mean \pm sem, $n = 2$ mice.

each mouse) (Figure 4.1). After a mouse had learned the novel third trial type, we introduced a fourth cue (triangle pattern) that required the mouse to turn the opposite direction of that required for the third cue (Figure 4.1 a). Mice learned the novel cue-response associations while maintaining high performance for the original two cue-response associations (Figure 4.1 b).

4.2.2 Rate of change during learning compared to stable behavior

We first asked whether the neuronal activity patterns were different between trials in which the mouse saw the novel cues and those in which it saw the familiar cues. Using a decoder based on population activity, the novel trial types were separable from the familiar trial types (Figure 4.1 c). These differences in activity between trial types could be visualized on a single day based on population activity in a dimensionality-reduced space (Figure 4.2 a). We quantified these differences in the full dimensional space throughout the duration of the task (Figure 4.2 b). We averaged these differences in activity between trial types across sessions for each mouse, again demonstrating the unique population activity that is specific

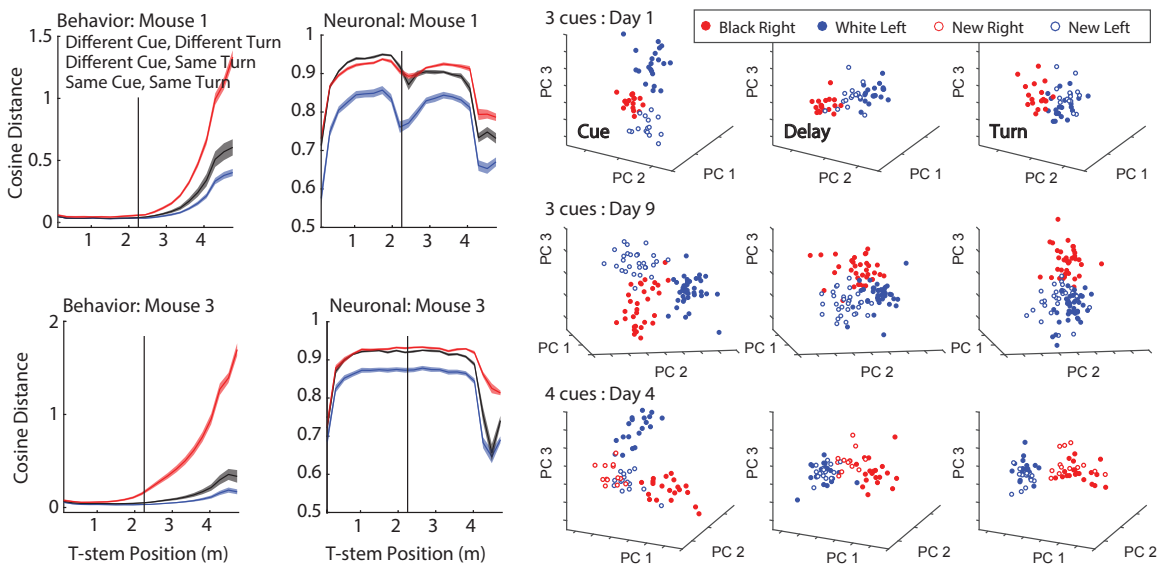


Figure 4.2 | Differences in activity between trial types. **a**, Cosine distance between single trial population vectors at each of 21 spatial bins spanning the duration of a trial. Cosine distance is computed within a given session for trials with the same cue, different cue but same turn, or different cue and different turn. Error bars indicate mean \pm sem, $n = 19$ sessions, 1 mouse. **b**, Example from a single mouse on the final day with four trial types. Top: Population activity during the cue period, delay period, and turn period in the same dimensionality reduced space. Each dot indicates a single trial.

to each mouse. We also quantified differences between trial types using the behavioral data.

Interestingly, we found differences in the running patterns of both mice for the same turn that was instructed by a different cue.

We tested if the addition of new learned associations altered the rate at which neuronal activity patterns changed during performance of previously learned trial types. We might expect learning to increase the rate of change as new information is incorporated into network activity. Surprisingly, we found that the rate of change was comparable between the days with stable performance of the two familiar trial types and during learning of the novel trial types (measured based on the performance of models of cells' activity-behavior relationships across days, as in (Figure 3.11) (Figure 4.3)).

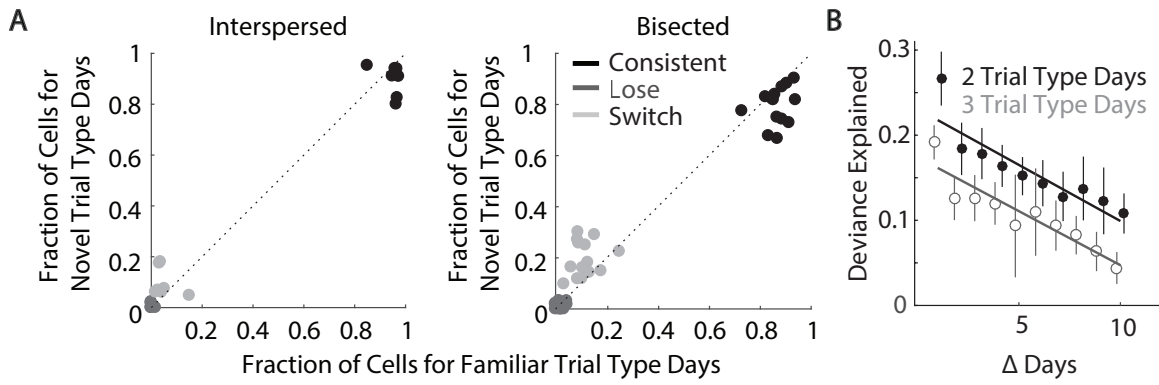


Figure 4.3 | a, For interspersed (left panel) and bisected groups (right panel), fraction of cells with, consistent (black), lost (medium gray), switched (light gray) activity-behavior relationships within one session based on our GLM analysis (see methods: GLM encoding model Analysis of model) on days with two familiar trial types and days with novel trial types. The interspersed group compares models that were built from interspersed chunks throughout the duration of the session and provides us with a baseline for change due to measurement noise. The bisected group compares models that were built from the first and second half of the session. **b,** For models fit to activity-behavior relationships on one day, the deviance explained of predictions of activity on other days. $p = 0.91$, ANOVA, comparing linear regression slopes for two trial type and novel trial type days.

4.2.3 Neurons with novel cue related activity

This similar rate of change could have occurred because the cells with activity related to the novel trial types were different from the cells with activity related to familiar trial types. We therefore analyzed if the cells with activity related to novel cues had activity related to familiar cues on previous days. Surprisingly, cells with activity related to novel cues were more likely to come from the group of cells which recently (within the past ten days) had activity related to the familiar cues than from a random sample of neurons (Figure ??).

The evolving pool of cells involved in representing task features was thus more likely to incorporate new task relevant information than the group of cells presently without task relevant information. This finding suggests that new information can be incorporated into the pool of task relevant activity as this pool continuously shifts over time, without disrupting baseline functionality. We speculate that the ability to incorporate new

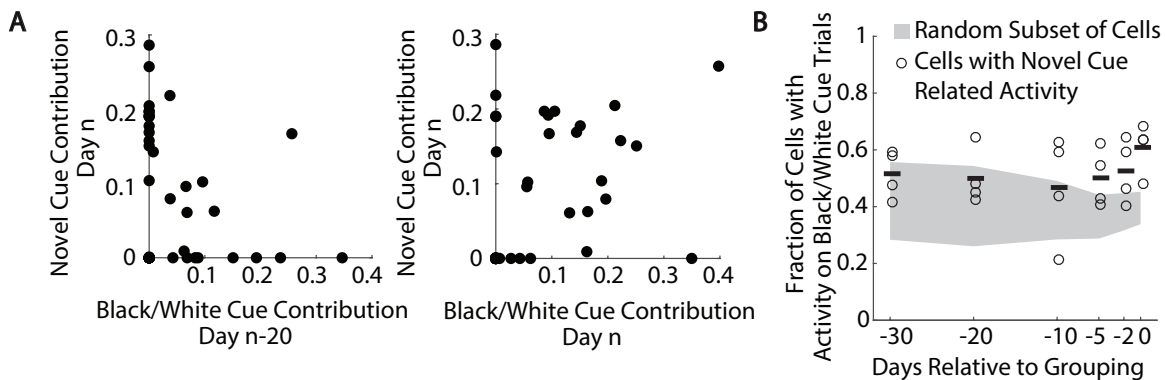


Figure 4.4 | Neurons with novel cue related activity came from the pool of cells with recent familiar cue related activity. **a,** Left: For individual cells in mouse 1, novel cue-related activity on day n (measured by > 0 contribution for novel cue onset/offset in the GLM, see Methods) vs. familiar cue-related activity on day n-20. Right: For the same cells, novel cue-related activity on day n vs familiar cue-related activity on day n. **b,** For cells with novel cue related activity on day n, the fraction of cells with activity related to either white or black cue onset/offset on the same day (day n) and on previous days (days n-2, n-5, n-10, n-20, n-30). Circles indicate individual data points and bars indicate mean, $n = 4$ (2 mice with 2 novel trial types each). Shaded region indicates 95 % confidence interval for the fraction of cells with activity on white cue-left turn and black cue-right turn trials taken from a random subset of neurons.

information using 'multitasking' neurons could allow for flexibility during learning, such that the network's ongoing changes provide a framework for the addition of new associations.

4.3 Discussion

We speculate that the changes in neuronal activity reported here reveal key features of how associations are formed and represented in PPC. In particular, our work reveals a potential strategy for a population of neurons to achieve stability in the maintenance of learned associations while also allowing flexibility to incorporate new information.

The rate of reorganization in neuronal activity-behavior relationships was only slightly elevated during learning compared to during stable task performance. We propose that

continuous reorganization of representations during stable behavior could endow the network with robustness to perturbations due to injury or learning of additional representations. Through the continuous exploration of parameter space for learned behaviors, the network can sample from the unconstrained space of possible solutions. Flexibility in the representation for a single task could allow the continuous addition of new representations without catastrophic forgetting of previously learned representations. These hypotheses must be tested explicitly in artificial systems. This could be done using an artificial neural network where there is no external controller to turn on and off learning. By continuously updating network connections during learning of a single task, this network could be made robust to change during learning of a second task.

4.3.1 Trial-trial variability is stable over learning

After controlling for behavioral choice, we found that neuronal activity patterns did not stabilize over the course of learning. This result is contradictory to a number of motor learning studies (Peters et al., 2014; Ganguly & Carmena, 2009). There are a few possible explanations for these conflicting results.

Emergence of stable patterns could be an artifact of increasing stereotypy of motor behaviors. (Peters et al., 2014) demonstrated that over the course of two weeks during learning of a cued lever press task, lever movements on individual trials became more stereotyped over time. Concurrently the number of movement related neurons went through a period of expansion and followed by contraction resulting in a smaller and more

stable population of movement-related neurons towards the end of learning. Similar results have been reported over the course of BMI control learning (Ganguly & Carmena, 2009). Our learning task was designed to control for change in the behavioral readout. By first training mice to report a learned stimulus-action pair with a learned behavioral response (left or right turn) before the acquisition of new stimulus-action relationships, we limit the amount of change in the behavioral response. We did not see a progressively stereotyped motor response over the course of the novel stimulus-action pairing. By closer inspection of the correlation matrices reported in these motor learning studies, it is clear that population responses become more similar during initial phases of learning, as motor responses become more stereotyped. However, after this initial phase of motor response learning, it is unclear whether the responses are completely stabilized or if they simply change at a slower rate. It will be important for future studies to control for behavioral change for the examination of neuronal change over learning.

Alternatively, the timescales over which learning occurs could vary across studies such that it is difficult to compare stabilization of neuronal responses. Our learning task simply requires the animal to match one of two possible actions to each novel stimulus. By learning through trial and error, it is possible for the animal to learn the new stimulus-action pair on a single trial. However, behavioral improvement over days suggests our animals are learning this behavior on a prolonged time scale. We see behavioral improvement over the course of four days during learning. (Peters et al., 2014) report learning of their lever press task over a similar time scale; therefore, it seems unlikely that differing timescales for learning

could explain differences in the stabilization of neuronal responses over time.

4.3.2 Steady number of task related neurons during learning

In contrast with previous studies in sensory and motor areas, we found the number of neurons with novel trial related activity to be stable over learning (Poort et al., 2015; Peters et al., 2014). Rather, from the very first introduction of the novel cues, there was already a large number of neurons with novel cue related activity. We could decode novel trial types from familiar trial types throughout the duration of the trial using neuronal population activity. Our ability to decode novel trial types was stable over learning, with only a slight rise over ten sessions (not a significant trend). These results suggest that the overrepresentation of familiar trial related activity was possibly transferred to novel cue representations. It will be of great interest in future studies to examine the extent to which familiar task representations can be transferred to the learning of novel tasks and the degree of task similarity required for the constructive transfer of these representations.

All of these measures for learning are likely dependent on task design and the brain region of interest. With newly available recording methods for tracking populations of cells over learning and over the course of stable behavior, it will be important to compare these measures across brain regions and across tasks.

4.4 Methods

4.4.1 Dimensionality reduction of neuronal and behavioral data

We reduced the dimensionality of single trial data into a space that captured the most variance across trial types and epochs of the trial. We performed principal component analysis (PCA) on averaged population responses across these different conditions. We constructed a data matrix X of size $N_{neurons} \times N_{conditions}$, in which columns corresponded to spatially binned z-scored population response vectors for a given segment of the trial (Figure 4.2 a). The principal components (PCs) of this data matrix were vectors v_a of length $N_{neurons}$ indexed by the number of PCs. For visualization, we then projected single trial data onto the first 3 PCs.

The motivation for this analysis was to visualize differences in single trial data that corresponded to differences in our conditions of interest. In Figure 4.4 we were interested in the evolving population activity throughout the duration of the trial for different trial types on a single day. Our neuronal data matrix X included 345 neurons identified on a single day and 7 spatial bins evenly spanning the duration of the trial for all 4 trial types (28 conditions). We projected single trial data onto the first 3 PCs of this matrix from individual spatial bins 1, 4 and 7 in the cue period, delay period and turn period. This analysis was solely for visualization. All quantified decoding was performed in the full dimensional space.

4.4.2 Cosine distance

Neuronal cosine distance was calculated from normalized population response vectors of all neurons that were identified on the session of interest ($1 \text{ spatial bin} \times N_{neurons}$). Behavioral cosine distance was calculated from normalized behavioral variable vectors (translational treadmill velocity, rotational treadmill velocity, view angle) ($1 \text{ spatial bin} \times 3 \text{ features}$).

Chapter 5

Discussion and future experiments

5.1 Dynamic reorganization of activity in cortex

Our work provides evidence that neuronal representations of behaviorally-relevant information undergo major changes over long time scales outside of the context of learning. In contrast to other studies in sensory and motor regions that reported no changes or subtle shifts in activity over a few days, our results revealed a major reorganization of neuronal activity patterns during a learned task over the course of weeks (Margolis et al., 2012; Peron et al., 2015b; Peters et al., 2014). For example, in HVC during birdsong, activity patterns had a 0.8 correlation coefficient over a five-day period (Liberti et al., 2016). In contrast, the changes we identified over long intervals approached those that could be expected by random reorganization. The magnitude of changes we observed appear consistent with those in hippocampal place cells upon repeated exposure to the same environment (Ziv et al., 2013). Our work demonstrates that the changing representations were likely used to perform the task, based on our inactivation results, which was not tested in chronic studies of hippocampal representations. It is important to

note that we found a wide range in the stability of encoding properties in single neurons. Although our decoding experiments revealed that information could be read out from the cells with the least consistent activity-behavior relationships, it will be important to test experimentally if downstream networks preferentially weight the inputs from the neurons with the most consistent relationships. This type of single cell perturbation experiment is now possible using all optical recording and stimulation techniques.

5.2 A strategy for maintaining and updating relevant activity

patterns

We speculate that the changes in neuronal activity reported here reveal key features of how associations are formed and represented in PPC. In particular, our work reveals a potential strategy for a population of neurons to achieve stability in the maintenance of learned associations while also allowing flexibility to incorporate new information. We illustrate this idea by focusing on activity patterns that separate one relevant task parameter, trial type. Over weeks, individual neurons did not maintain different activity between trial types, such that many neurons gained or lost selectivity and a small fraction of neurons switched trial type preferences. Despite these seemingly random changes over weeks, information about trial type could be read out at above chance levels from the population using a single decoder. The decoder's success was because the majority of neurons did not change in a way that their activity had opposite implications for a decoder on different days. That is, most neurons that had higher activity on black cue-right turn

trials eventually lost selectivity and less frequently switched to having higher activity on white cue-left turn trials at the same location in the maze. Many changes therefore occurred in a null dimension relative to the dimension important for trial type (Ajemian et al., 2013; Rokni et al., 2007). Importantly, these changes need not be coordinated in an 'intelligent' or 'structured' way to occur specifically in a null dimension. Rather, this effect is characteristic of a high dimensional activity space because in high dimensional spaces most dimensions are orthogonal to each other. Most random change in neuronal representations would thus occur in an orthogonal dimension to the one relevant for reading out trial type (Buonomano & Maass, 2009). We note, however, that more information would be accessible to the readout if it functioned as a dynamically adaptive decoder. It is possible that over long timescales an ideal decoder could also slowly drift in response to the dynamically encoded information, but could change at a slower pace. In such a case, the readout network could have a lag in its changes and/or a slower rate of change, afforded by the properties of a high dimensional space where drift in any direction will often occur in an orthogonal direction to the optimal decision boundary. Over long timescales, learned associations that are not practiced could be lost if the readout is not updated for an extended interval. On the other hand, learned associations that are often practiced could maintain a tight link between drifting activity patterns and the relevant readout. Importantly, a slow drift, such as could be produced by background synaptic plasticity, has been shown to provide computational advantages such as avoiding local minima and providing exploratory strategies described in the field of reinforcement

learning (Kappel et al., 2015; Yu et al., 2016). In this framework, neuronal activity is continuously remodeled in order to maintain the most up-to-date, relevant information for behavior while discarding irrelevant, previously learned memories over long timescales.

5.3 Balancing stability and flexibility according to role

The importance of representations that mediate a tradeoff between stability and flexibility likely varies depending on the function of the population of neurons. In areas closely connected to sensory coding or the generation of motor actions, there may be a greater need for stability and less need for plasticity, which could explain why studies of sensory and motor cortex have described less drastic changes than those we report. However, it will be important to test the stability of sensory and motor representations over time windows similar to those we used here. We focused on the PPC, which receives multisensory input, has recurrent connections with frontal regions, and has outputs to motor-related structures, suggesting that it is an association area (Harvey et al., 2012; Oh et al., 2014). Our previous work found little evidence of purely visual responses in PPC during passive viewing, suggesting that its activity is not driven solely by sensory input (Harvey et al., 2012). Also, PPC is multiple synapses from movement-generating regions, such that it is unlikely important for directly driving actions. In contrast to sensory and motor regions, association regions, like the PPC, probably require flexibility for learned behaviors as one of their key properties, in which case malleable activity patterns in neuronal populations would be highly advantageous. Consistent with this idea, studies of

the turnover rate of dendritic spines have revealed that spines in another association region, hippocampus, turn over at a faster rate than those in primary somatosensory cortex and have a much lower percentage of stable spines (Attardo et al., 2015). Analogous to learning new information in association areas on top of stable sensory and motor representations, work in artificial networks has demonstrated the utility of training additional layers on top of previously learned deep nets to perform complex tasks (Kümmerer et al., 2014). It will be of interest to directly compare the rates of activity changes in populations of neurons across different brain regions, including in cortical and subcortical areas, to test if abstract learned representations drift at faster rates than activity patterns that represent sensory stimuli or generate motor actions.

5.4 Stability in the emergent properties of the network

Our work provides evidence that individual PPC neurons do not have specified roles in network activity. Instead, not only did we observe that neurons lost or gained activity-behavior relationships over time, but we also found some neurons that switched their activity-behavior relationships, suggesting that they provided different information to the network at different time points in their lifetime. We found that neuronal activity was best described by combinations of behaviorally relevant features similar to recent work suggesting information in cortical neurons is multiplexed, such that neurons participate in many information channels (Cromer et al., 2010; Rigotti et al., 2013). In addition, the changes in activity we observed suggest that a neuron's activity might not be confined to a

specific class of activity pattern, thus supporting recent evidence for category-free neuronal populations in the rodent PPC (Raposo et al., 2014). Together our work and others suggest that the role of individual neurons could be less important than the overall population activity pattern, such that individual neurons participate in many information streams and can change their participation over time (Yuste, 2015). Consistent with this idea, we identified that although the activity-behavior relationships of individual neurons changed over time, the PPC population activity had similar statistics of activity on each day, using different neurons or the same neurons in different ways. This result suggests that the population activity reached a set point of activity that was necessary for the PPC’s role in the task. This idea is conceptually similar to the homeostatic ideas that have been revealed in the stomatogastric ganglion (Marder, 2011; O’Leary et al., 2014; Prinz et al., 2004). In that system, innovative work has revealed that the same firing patterns of neurons can be achieved through different combinations of ion channels and ion channel expression levels. We speculate that a similar idea could be present in neuronal populations given the underlying changing activity of individual neurons.

References

- Abbott, L. & Sussillo, D. (2009). Generating Coherent Patterns of Activity from Chaotic Neural Networks. *Neuron*, 63(4), 544–557.
- Ajemian, R., D'Ausilio, A., Moorman, H., & Bizzi, E. (2013). A theory for how sensorimotor skills are learned and retained in noisy and nonstationary neural circuits. *Proceedings of the National Academy of Sciences of the United States of America*, 110(52), E5078–87.
- Andermann, M. L., Kerlin, A. M., & Reid, C. (2010). Chronic cellular imaging of mouse visual cortex during operant behavior and passive viewing. *Frontiers in Cellular Neuroscience*, 4, 3.
- Andersen, R. A. & Cui, H. (2009). Intention, action planning, and decision making in parietal-frontal circuits. *Neuron*, 63(5), 568–583.
- Aronov, D. & Tank, D. W. (2014). Engagement of Neural Circuits Underlying 2D Spatial Navigation in a Rodent Virtual Reality System. *Neuron*, 84(2), 442–456.
- Attardo, A., Fitzgerald, J. E., & Schnitzer, M. J. (2015). Impermanence of dendritic spines in live adult CA1 hippocampus. *Nature*, 523(7562), 592–6.
- Barash, S., Bracewell, R. M., Fogassi, L., Gnadt, J. W., & Andersen, R. A. (1991). Saccade-related activity in the lateral intraparietal area. I. Temporal properties; comparison with area 7a. *Journal of Neurophysiology*, 66(3), 1095–1108.
- Batista, A. P., Buneo, C. A., Snyder, L. H., & Andersen, R. A. (1999). Reach plans in eye-centered coordinates. *Science*, 285(5425), 257–260.
- Berridge, M. J., Lipp, P., & Bootman, M. D. (2000). The versatility and universality of calcium signalling. *Nature Reviews Molecular Cell Biology*, 1(1), 11–21.

- Berryhill, M. E. & Olson, I. R. (2008). The right parietal lobe is critical for visual working memory. *Neuropsychologia*, 46(7), 1767–1774.
- Bisley, J. W. & Goldberg, M. E. (2010). Attention, intention, and priority in the parietal lobe. *Annual review of neuroscience*, 33, 1–21.
- Buonomano, D. V. (2005). A learning rule for the emergence of stable dynamics and timing in recurrent networks. *Journal of neurophysiology*, 94(4), 2275–83.
- Buonomano, D. V. & Maass, W. (2009). State-dependent computations: spatiotemporal processing in cortical networks. *Nature Reviews Neuroscience*, 10(2), 113–125.
- Chen, T.-W., Wardill, T. J., Sun, Y., Pulver, S. R., Renninger, S. L., Baohan, A., Schreiter, E. R., Kerr, R. a., Orger, M. B., Jayaraman, V., Looger, L. L., Svoboda, K., & Kim, D. S. (2013). Ultrasensitive fluorescent proteins for imaging neuronal activity. *Nature*, 499(7458), 295–300.
- Chestek, C. A., Batista, A. P., Santhanam, G., Yu, B. M., Afshar, A., Cunningham, J. P., Gilja, V., Ryu, S. I., Churchland, M. M., & Shenoy, K. V. (2007). Single-neuron stability during repeated reaching in macaque premotor cortex. *The Journal of neuroscience : the official journal of the Society for Neuroscience*, 27(40), 10742–50.
- Constantinidis, C. (2006). Posterior parietal mechanisms of visual attention. *Reviews in the Neurosciences*, 17(4), 415–427.
- Constantinidis, C., Forest, W., Carolina, N., Inserm, U., & Fédératif, I. (2004). The primate working memory networks EXPERIMENTAL INVESTIGATION OF. *Behavioral Neuroscience*, 4(4), 444–465.
- Constantinidis, C. & Steinmetz, M. A. (1996). Neuronal activity in posterior parietal area 7a during the delay periods of a spatial memory task. *Journal of Neurophysiology*, 76(2), 1352–1355.
- Cromer, J. A., Roy, J. E., & Miller, E. K. (2010). Representation of multiple, independent categories in the primate prefrontal cortex. *Neuron*, 66(5), 796–807.

- Darian-Smith, C. & Gilbert, C. (1994). Axonal sprouting accompanies functional reorganization in adult cat striate cortex. *Nature*.
- Denk, W., Strickler, J. H., & Webb, W. W. (1990). Two-photon laser scanning fluorescence microscopy. *Science (New York, N.Y.)*, 248(4951), 73–6.
- Dombeck, D. A., Harvey, C. D., Tian, L., Looger, L. L., & Tank, D. W. (2010). Functional imaging of hippocampal place cells at cellular resolution during virtual navigation. *Nature Neuroscience*, 13(11), 1433–1440.
- Dorand, R. D., Barkauskas, D. S., Evans, T. A., Petrosiute, A., & Huang, A. Y. (2014). Comparison of intravital thinned skull and cranial window approaches to study CNS immunobiology in the mouse cortex. *Intravital*, 3(2).
- Ebbinghaus, H. (1880). *Ueber das Gedächtnis*. Passavia Universitatsverlag, 1983, volume 1 o edition.
- Freedman, D. J. & Assad, J. A. (2006). Experience-dependent representation of visual categories in parietal cortex. *Nature*, 443(7107), 85–88.
- Freedman, D. J. & Assad, J. A. (2009). Distinct encoding of spatial and nonspatial visual information in parietal cortex. *Journal of Neuroscience*, 29(17), 5671–5680.
- Freedman, D. J. & Assad, J. A. (2016). Neuronal Mechanisms of Visual Categorization: An Abstract View on Decision Making. *Annual review of neuroscience*, 39, 129–47.
- Friedman, J., Hastie, T., & Tibshirani, R. (2010). Regularization Paths for Generalized Linear Models via Coordinate Descent. *Journal of statistical software*, 33(1), 1–22.
- Gallese, V., Murata, A., Kaseda, M., Niki, N., & Sakata, H. (1994). Deficit of hand preshaping after muscimol injection in monkey parietal cortex. *NeuroReport*, 5(12), 1525–9.
- Ganguly, K. & Carmena, J. M. (2009). Emergence of a Stable Cortical Map for Neuroprosthetic Control. *PLoS Biology*, 7(7), e1000153.

- Garrett, M. E., Nauhaus, I., Marshel, J. H., & Callaway, E. M. (2014). Topography and Areal Organization of Mouse Visual Cortex. *Journal of Neuroscience*, 34(37), 12587–12600.
- Gilbert, C. & Wiesel, T. (1992). Receptive field dynamics in adult primary visual cortex. *Nature*.
- Gilbert, C. D. & Wiesel, T. N. (1990). The influence of contextual stimuli on the orientation selectivity of cells in primary visual cortex of the cat. *Vision research*, 30(11), 1689–701.
- Goard, M. J., Pho, G. N., Woodson, J., & Sur, M. (2016). Distinct roles of visual, parietal, and frontal motor cortices in memory-guided sensorimotor decisions. *eLife*, 5, 471–477.
- Goldey, G. J., Roumis, D. K., Glickfeld, L. L., Kerlin, A. M., Reid, R. C., Bonin, V., Schafer, D. P., & Andermann, M. L. (2014). Removable cranial windows for long-term imaging in awake mice. *Nature protocols*, 9(11), 2515–38.
- Goodale, M. A. & Milner, A. D. (1992). Separate visual pathways for perception and action. *Trends in Neurosciences*, 15(1), 20–5.
- Greenberg, D. S. & Kerr, J. N. D. (2009). Automated correction of fast motion artifacts for two-photon imaging of awake animals. *Journal of Neuroscience Methods*, 176(1), 1–15.
- Haaland, K. Y., Harrington, D. L., & Knight, R. T. (2000). Neural representations of skilled movement. *Brain: A journal of neurology*, 123 (Pt 1(11)), 2306–2313.
- Hamel, E., Grewe, B., Parker, J., & Schnitzer, M. (2015). Cellular Level Brain Imaging in Behaving Mammals: An Engineering Approach. *Neuron*, 86(1), 140–159.
- Harvey, C. D., Coen, P., & Tank, D. W. (2012). Choice-specific sequences in parietal cortex during a virtual-navigation decision task. *Nature*, 484(7392), 62–68.
- Harvey, C. D., Collman, F., Dombeck, D. A., & Tank, D. W. (2009). Intracellular dynamics of hippocampal place cells during virtual navigation. *Nature*, 461(7266), 941–6.

- Hofer, S. B., Mrsic-Flogel, T. D., Bonhoeffer, T., & Hübener, M. (2006). Prior experience enhances plasticity in adult visual cortex. *Nature Neuroscience*, 9(1), 127–132.
- Hofer, S. B., Mrsic-Flogel, T. D., Bonhoeffer, T., & Hübener, M. (2009). Experience leaves a lasting structural trace in cortical circuits. *Nature*, 457(7227), 313–317.
- Huber, D., Gutnisky, D. a., Peron, S., O'Connor, D. H., Wiegert, J. S., Tian, L., Oertner, T. G., Looger, L. L., & Svoboda, K. (2012). Multiple dynamic representations in the motor cortex during sensorimotor learning. *Nature*, 484(7395), 473–8.
- Kaas, J. H., Krubitzer, L. A., Chino, Y. M., Langston, A. L., Polley, E. H., & Blair, N. (1990). Reorganization of retinotopic cortical maps in adult mammals after lesions of the retina. *Science (New York, N.Y.)*, 248(4952), 229–31.
- Kalatsky, V. A. & Stryker, M. P. (2003). New paradigm for optical imaging: temporally encoded maps of intrinsic signal. *Neuron*, 38(4), 529–45.
- Kappel, D., Habenschuss, S., Legenstein, R., & Maass, W. (2015). Network Plasticity as Bayesian Inference. *PLoS computational biology*, 11(11), e1004485.
- Kentros, C. G., Agnihotri, N. T., Streater, S., Hawkins, R. D., & Kandel, E. R. (2004). Increased Attention to Spatial Context Increases Both Place Field Stability and Spatial Memory. *Neuron*, 42(2), 283–295.
- Komiyama, T., Sato, T. R., O'Connor, D. H., Zhang, Y.-X., Huber, D., Hooks, B. M., Gabitto, M., & Svoboda, K. (2010). Learning-related fine-scale specificity imaged in motor cortex circuits of behaving mice. *Nature*, 464(7292), 1182–1186.
- Kümmerer, M., Theis, L., & Bethge, M. (2014). Deep Gaze I: Boosting Saliency Prediction with Feature Maps Trained on ImageNet.
- LeCun, Y., Bengio, Y., & Hinton, G. (2015). Deep learning. *Nature*, 521(7553), 436–44.
- Liberti, W. A., Markowitz, J. E., Perkins, L. N., Liberti, D. C., Leman, D. P., Guitchounts, G., Velho, T., Kotton, D. N., Lois, C., & Gardner, T. J. (2016). Unstable neurons underlie

a stable learned behavior. *Nature neuroscience*, advance on.

Licata, A. M., Kaufman, M. T., Raposo, D., Ryan, M. B., Sheppard, J. P., & Churchland, A. K. (2016). Posterior parietal cortex guides visual decisions in rats. *bioRxiv*, (pp. 066639).

Makino, H. & Komiyama, T. (2015). Learning enhances the relative impact of top-down processing in the visual cortex. *Nature neuroscience*.

Mank, M., Santos, A. F., Direnberger, S., Mrsic-Flogel, T. D., Hofer, S. B., Stein, V., Hendel, T., Reiff, D. F., Levelt, C., Borst, A., Bonhoeffer, T., Hübener, M., & Griesbeck, O. (2008). A genetically encoded calcium indicator for chronic *in vivo* two-photon imaging. *Nature methods*, 5(9), 805–811.

Marder, E. (2011). Variability, compensation, and modulation in neurons and circuits. *Proceedings of the National Academy of Sciences of the United States of America*, (Supplement 3), 15542–8.

Margolis, D. J., Lütcke, H., Schulz, K., Haiss, F., Weber, B., Kügler, S., Hasan, M. T., & Helmchen, F. (2012). Reorganization of cortical population activity imaged throughout long-term sensory deprivation. *Nature Neuroscience*, 15(11), 1539–1546.

Marshel, J. H., Garrett, M. E., Nauhaus, I., & Callaway, E. M. (2011). Functional specialization of seven mouse visual cortical areas. *Neuron*, 72(6), 1040–54.

McNaughton, B. L., Mizumori, S. J. Y., Barnes, C. A., Leonard, B. J., Marquis, M., & Green, E. J. (1994). Cortical Representation of Motion during Unrestrained Spatial Navigation in the Rat. *Cerebral Cortex*, 4(1), 27–39.

Merzenich, M. M., Nelson, R. J., Stryker, M. P., Cynader, M. S., Schoppmann, A., & Zook, J. M. (1984). Somatosensory cortical map changes following digit amputation in adult monkeys. *The Journal of Comparative Neurology*, 224(4), 591–605.

Messinger, A., Squire, L. R., Zola, S. M., & Albright, T. D. (2001). Neuronal representations of stimulus associations develop in the temporal lobe during learning. *Proceedings of the National Academy of Sciences of the United States of America*, 98(21), 12239–44.

- Morcos, A. S. & Harvey, C. D. (2016). History-dependent variability in population dynamics during evidence accumulation in cortex. *Nature Neuroscience*, 19(12), 1672–1681.
- Nitz, D. A. (2006). Tracking Route Progression in the Posterior Parietal Cortex. *Neuron*, 49(5), 747–756.
- O'Connor, D. H., Huber, D., & Svoboda, K. (2009). Reverse engineering the mouse brain. *Nature*, 461(7266), 923–929.
- Oh, S. W., Harris, J. A., Ng, L., Winslow, B., Cain, N., Mihalas, S., Wang, Q., Lau, C., Kuan, L., Henry, A. M., Mortrud, M. T., Ouellette, B., Nguyen, T. N., Sorensen, S. A., Slaughterbeck, C. R., Wakeman, W., Li, Y., Feng, D., Ho, A., Nicholas, E., Hirokawa, K. E., Bohn, P., Joines, K. M., Peng, H., Hawrylycz, M. J., Phillips, J. W., Hohmann, J. G., Wohnoutka, P., Gerfen, C. R., Koch, C., Bernard, A., Dang, C., Jones, A. R., & Zeng, H. (2014). A mesoscale connectome of the mouse brain. *Nature*, 508(7495), 207–214.
- Oheim, M., Beaurepaire, E., Chaigneau, E., Mertz, J., & Charpak, S. (2001). Two-photon microscopy in brain tissue: parameters influencing the imaging depth. *Journal of neuroscience methods*, 111(1), 29–37.
- O'Leary, T., Williams, A., Franci, A., & Marder, E. (2014). Cell Types, Network Homeostasis, and Pathological Compensation from a Biologically Plausible Ion Channel Expression Model. *Neuron*, 82(4), 809–821.
- Otchy, T. M., Wolff, S. B. E., Rhee, J. Y., Pehlevan, C., Kawai, R., Kempf, A., Gobes, S. M. H., & Ölveczky, B. P. (2015). Acute off-target effects of neural circuit manipulations. *Nature*, 528(7582), 358–363.
- Padoa-Schioppa, C., Li, C.-S. R., & Bizzi, E. (2004). Neuronal activity in the supplementary motor area of monkeys adapting to a new dynamic environment. *Journal of neurophysiology*, 91(1), 449–73.
- Park, I. M., Meister, M. L. R., Huk, A. C., & Pillow, J. W. (2014). Encoding and decoding in parietal cortex during sensorimotor decision-making. *Nature Neuroscience*, 17(10), 1395–1403.

- Peron, S., Chen, T.-W., & Svoboda, K. (2015a). Comprehensive imaging of cortical networks. *Current Opinion in Neurobiology*, 32, 115–123.
- Peron, S., Freeman, J., Iyer, V., Guo, C., & Svoboda, K. (2015b). A Cellular Resolution Map of Barrel Cortex Activity during Tactile Behavior. *Neuron*.
- Peters, A. J., Chen, S. X., & Komiyama, T. (2014). Emergence of reproducible spatiotemporal activity during motor learning. *Nature*, 510(7504), 263–7.
- Pologruto, T. A., Sabatini, B. L., & Svoboda, K. (2003). ScanImage: flexible software for operating laser scanning microscopes. *Biomedical engineering online*, 2(1), 13.
- Poort, J., Khan, A. G., Pachitariu, M., Nemri, A., Orsolic, I., Krupic, J., Bauza, M., Sahani, M., Keller, G. B., Mrsic-Flogel, T. D., & Hofer, S. B. (2015). Learning Enhances Sensory and Multiple Non-sensory Representations in Primary Visual Cortex. *Neuron*, 86(6), 1478–90.
- Prinz, A. A., Bucher, D., & Marder, E. (2004). Similar network activity from disparate circuit parameters. *Nature Neuroscience*, 7(12), 1345–1352.
- Raposo, D., Kaufman, M. T., & Churchland, A. K. (2014). A category-free neural population supports evolving demands during decision-making. *Nature neuroscience*, 17(12), 1784–92.
- Ratzlaff, E. H. & Grinvald, A. (1991). A tandem-lens epifluorescence macroscope: hundred-fold brightness advantage for wide-field imaging. *Journal of neuroscience methods*, 36(2-3), 127–37.
- Rawley, J. B. & Constantinidis, C. (2009). Neural correlates of learning and working memory in the primate posterior parietal cortex. *Neurobiology of Learning and Memory*, 91(2), 129–138.
- Rigotti, M., Barak, O., Warden, M. R., Wang, X.-J., Daw, N. D., Miller, E. K., & Fusi, S. (2013). The importance of mixed selectivity in complex cognitive tasks. *Nature*, 497(7451), 585–590.

- Robertson, D. & Irvine, D. R. F. (1989). Plasticity of frequency organization in auditory cortex of guinea pigs with partial unilateral deafness. *The Journal of Comparative Neurology*, 282(3), 456–471.
- Rokni, U., Richardson, A. G., Bizzi, E., & Seung, H. S. (2007). Motor Learning with Unstable Neural Representations. *Neuron*, 54(4), 653–666.
- Rose, T., Jaepel, J., Hübener, M., & Bonhoeffer, T. (2016). Cell-specific restoration of stimulus preference after monocular deprivation in the visual cortex. *Science*, 352(6291).
- Rushworth, M. F., Nixon, P. D., Wade, D. T., Renowden, S., & Passingham, R. E. (1998). The left hemisphere and the selection of learned actions. *Neuropsychologia*, 36(1), 11–24.
- Sakai, K. & Miyashita, Y. (1991). Neural organization for the long-term memory of paired associates. *Nature*, 354(6349), 152–5.
- Seal, J. (1989). Sensory and motor functions of the superior parietal cortex of the monkey as revealed by single-neuron recordings. *Brain behavior and evolution*, 33(2-3), 113–117.
- Shi, J. & Malik, J. (2000). Normalized cuts and image segmentation. *IEEE Transactions on Pattern Analysis and Machine Intelligence*, 22(8), 888–905.
- Stettler, D. D., Yamahachi, H., Li, W., Denk, W., & Gilbert, C. D. (2006). Axons and synaptic boutons are highly dynamic in adult visual cortex. *Neuron*, 49(6), 877–87.
- Stevenson, I. H., Cherian, A., London, B. M., Sachs, N. A., Lindberg, E., Reimer, J., Slutzky, M. W., Hatsopoulos, N. G., Miller, L. E., & Kording, K. P. (2011). Statistical assessment of the stability of neural movement representations. *Journal of Neurophysiology*, 106(2).
- Stricanne, B., Andersen, R. A., & Mazzoni, P. (1996). Eye-centered, head-centered, and intermediate coding of remembered sound locations in area LIP. *Journal of Neurophysiology*, 76(3), 2071–2076.
- Theer, P., Hasan, M. T., & Denk, W. (2003). Two-photon imaging to a depth of 1000 microm

in living brains by use of a Ti:Al₂O₃ regenerative amplifier. *Optics letters*, 28(12), 1022–4.

Tian, L., Hires, S. A., Mao, T., Huber, D., Chiappe, M. E., Chalasani, S. H., Petreanu, L., Akerboom, J., McKinney, S. A., Schreiter, E. R., Bargmann, C. I., Jayaraman, V., Svoboda, K., & Looger, L. L. (2009). Imaging neural activity in worms, flies and mice with improved GCaMP calcium indicators. *Nature Methods*, 6(12), 875–881.

Tolias, A. S., Ecker, A. S., Siapas, A. G., Hoenselaar, A., Keliris, G. A., & Logothetis, N. K. (2007). Recording Chronically From the Same Neurons in Awake, Behaving Primates. *Journal of Neurophysiology*, 98(6), 3780–3790.

Tonegawa, S., Liu, X., Ramirez, S., & Redondo, R. (2015). Memory Engram Cells Have Come of Age. *Neuron*, 87(5), 918–931.

Trachtenberg, J. T., Chen, B. E., Knott, G. W., Feng, G., Sanes, J. R., Welker, E., & Svoboda, K. (2002). Long-term in vivo imaging of experience-dependent synaptic plasticity in adult cortex. *Nature*, 420(6917), 788–794.

Veit, L., Pidpruzhnykova, G., & Nieder, A. (2015). Associative learning rapidly establishes neuronal representations of upcoming behavioral choices in crows. *Proceedings of the National Academy of Sciences of the United States of America*, 112(49), 15208–13.

Vogelstein, J. T., Packer, A. M., Machado, T. a., Sippy, T., Babadi, B., Yuste, R., & Paninski, L. (2010). Fast nonnegative deconvolution for spike train inference from population calcium imaging. *Journal of neurophysiology*, 104(6), 3691–3704.

Wang, Q. & Burkhalter, A. (2007). Area map of mouse visual cortex. *The Journal of Comparative Neurology*, 502(3), 339–357.

Whitlock, J. R., Pfuhl, G., Dagslott, N., Moser, M.-B., & Moser, E. I. (2012). Functional Split between Parietal and Entorhinal Cortices in the Rat. *Neuron*, 73(4), 789–802.

Xu, H.-T., Pan, F., Yang, G., & Gan, W.-B. (2007). Choice of cranial window type for in vivo imaging affects dendritic spine turnover in the cortex. *Nature Neuroscience*, 10(5), 549–551.

Yang, G., Pan, F., Parkhurst, C. N., Grutzendler, J., & Gan, W.-B. (2010). Thinned-skull cranial window technique for long-term imaging of the cortex in live mice. *Nature Protocols*, 5(2), 201–208.

Yaroslavsky, A. N., Schulze, P. C., Yaroslavsky, I. V., Schober, R., Ulrich, F., & Schwarzmaier, H. J. (2002). Optical properties of selected native and coagulated human brain tissues in vitro in the visible and near infrared spectral range. *Physics in medicine and biology*, 47(12), 2059–73.

Yu, Z., Kappel, D., Legenstein, R., Song, S., Chen, F., & Maass, W. (2016). CaMKII activation supports reward-based neural network optimization through Hamiltonian sampling.

Yuste, R. (2015). From the neuron doctrine to neural networks. *Nature Reviews Neuroscience*, 16(8), 487–497.

Zipfel, W. R., Williams, R. M., & Webb, W. W. (2003). Nonlinear magic: multiphoton microscopy in the biosciences. *Nature Biotechnology*, 21(11), 1369–1377.

Ziv, Y., Burns, L. D., Cocker, E. D., Hamel, E. O., Ghosh, K. K., Kitch, L. J., El Gamal, A., & Schnitzer, M. J. (2013). Long-term dynamics of CA1 hippocampal place codes. *Nature neuroscience*, 16(3), 264–6.